frontiers in Environmental Science

TYPE Original Research
PUBLISHED 20 April 2026
DOI 10.3389/fenvs.2026.1777634

OPEN ACCESS

EDITED BY
Markus Schaffert,
Hochschule Mainz, Germany

REVIEWED BY
Luan Marca,
Pontifical Catholic University of Rio Grande do Sul, Brazil
Dogbo Sedoami Flora,
Université d'Abomey-Calavi, Benin

*CORRESPONDENCE
Jhon A. Zabaleta-Santisteban,
jhon.zabaleta.epg@untrm.edu.pe
Elgar Barboza,
elgar.barboza@untrm.edu.pe

RECEIVED 29 December 2025
REVISED 17 February 2026
ACCEPTED 19 February 2026
PUBLISHED 20 April 2026

CITATION
Zabaleta-Santisteban JA, Rojas-Briceño NB, Silva-López JO, Medina-Medina AJ, Tuesta-Trauco KM, Rivera-Fernandez AS, Silva-Melendez TB, Grandez-Alberca MA, Puscan-Rojas J, Salas López R, Oliva-Cruz M, Cotrina-Sanchez A, Gómez-Fernández D and Barboza E (2026) Mapping current and future coffee suitability in Peru under climate change: implications for restoration and deforestation-free development.
Front. Environ. Sci. 14:1777634.
doi: 10.3389/fenvs.2026.1777634

Mapping current and future coffee suitability in Peru under climate change: implications for restoration and deforestation-free development

Jhon A. Zabaleta-Santisteban[1]*, Nilton B. Rojas-Briceño[2], Jhonsy O. Silva-López[3], Angel J. Medina-Medina[1], Katerin M. Tuesta-Trauco[1], Abner S. Rivera-Fernandez[1], Teodoro B. Silva-Melendez[1], Marlen A. Grandez-Alberca[1], Julio Puscan-Rojas[1], Rolando Salas López[1], Manuel Oliva-Cruz[1], Alexander Cotrina-Sanchez[1], Darwin Gómez-Fernández[4] and Elgar Barboza[1]*

[1]Instituto de Investigación para el Desarrollo Sustentable de Ceja de Selva (INDES-CES), Universidad Nacional Toribio Rodríguez de Mendoza de Amazonas, Chachapoyas, Peru, [2]Grupo de Investigación en Ciencia de la Información Geoespacial (CIGEO), Escuela Profesional de Ingeniería Ambiental, Universidad Nacional de Moquegua, Pacocha, Peru, [3]Área de cartografía y teledetección, Laboratorio de Agrostología, Instituto de Investigación en Ganadería y Biotecnología, Facultad de Ingeniería Zootecnista, Agronegocios y Biotecnología, Universidad Nacional Toribio Rodríguez de Mendoza de Amazonas, Chachapoyas, Peru, [4]Centro Experimental Yanayacu, Dirección de Servicios Estratégicos Agrarios (DSEA), Instituto Nacional de Innovación Agraria (INIA), Cajamarca, Peru

Coffee cultivation is central to rural livelihoods and Andean–Amazonian landscapes in Peru; however, it faces increasing pressure from climate change and land-use restrictions. This study aimed to assess the current and future ecological suitability of Coffea arabica at the national scale. A Maximum Entropy (MaxEnt) modeling framework was applied, integrating high-resolution bioclimatic, topographic, and edaphic variables. Model performance was robust (mean AUC = 0.858), and variable importance was evaluated using jackknife tests and contribution metrics. Elevation, precipitation of the driest quarter (bio17), soil nitrogen content, and bulk density were identified as the main determinants of habitat suitability. Under current climatic conditions, highly suitable areas cover 42,322.95 km2 (3.3% of Peru), mainly along the eastern Andean slopes. Spatial exclusion scenarios revealed a pronounced funnel effect in effective land availability, with reductions exceeding 80% when forest-cover constraints were applied. Approximately 39.8% of highly suitable areas overlap with degraded lands, highlighting opportunities for productive restoration through agroforestry systems. Future projections under SSP1–2.6 to SSP5–8.5 scenarios indicate consistent contractions of highly suitable areas (−23% to −42%) and an upslope shift toward higher elevations, while unsuitable areas expand by 4%–5% nationally. These findings provide spatially explicit evidence to support climate-smart territorial planning, restoration prioritization, and sustainable coffee development under accelerating climate change.

KEYWORDS
agroclimatic suitability, climate change, ecological modeling, potential distribution, SSP

1 Introduction

Coffee occupies a strategic position within the global agri-food system and plays a central role in international trade, constituting one of the most important agricultural commodities worldwide (Bilen et al., 2023; Koutouleas et al., 2022; Liu et al., 2025). It is cultivated in more than 80 tropical countries and provides livelihoods for millions of people, including approximately 25 million producers, most of whom are smallholder farmers (Alberto et al., 2024; Lahai et al., 2025). Global coffee production is dominated by *Coffea arabica* and *Coffea canephora*, with *C. arabica* being the most widely distributed and consumed species, accounting for nearly 70% of total global production (Beche et al., 2024; Liu et al., 2025; Parada-Molina et al., 2025). Nevertheless, *C. arabica* is considered particularly vulnerable to climate change due to its narrow physiological tolerance ranges to temperature and water availability (Ovalle-Rivera et al., 2015; Parada-Molina et al., 2025).

The production of *C. arabica* depends on specific agroecological conditions, including altitude, temperature, precipitation, soil properties, and agronomic management practices, all of which directly influence both yield and the sensory quality of coffee beans (Abdelwahab et al., 2024; Haro et al., 2025). Scientific evidence indicates that these determinants are highly sensitive to climate change, posing a growing challenge to the long-term sustainability of coffee production systems at the global scale (Intergovernmental Panel on Climate Change [PCC], 2022; Jiang et al., 2020; Mendes et al., 2022). In particular, increasing mean temperatures and altered precipitation regimes are driving upslope shifts of agroclimatically suitable zones and a progressive contraction of optimal areas in lowland regions (Hou et al., 2025; Ovalle-Rivera et al., 2015).

In tropical America, especially in Mesoamerica and the Andean region, the impacts of climate change on coffee production are expected to be particularly severe, manifesting as increased water stress, higher incidence of pests and diseases, and growing production instability (Avelino et al., 2015; Campos-Trigoso A. et al., 2025; Chemura et al., 2021). Adaptation of perennial crops such as coffee is especially complex due to their long production cycles and the long-term consequences associated with agronomic and land-use decisions (de Sousa et al., 2019). In this context, practices such as agroforestry, sustainable soil management, and the adoption of heat- and drought-tolerant varieties have been widely recognized as key climate adaptation strategies (Attiogbé et al., 2022; Griscom et al., 2017).

Peru, characterized by pronounced climatic and topographic heterogeneity, concentrates its coffee production mainly along the eastern slopes of the Andes, within the Andean–Amazonian corridor. This territorial configuration generates strong altitudinal and microclimatic gradients that increase crop sensitivity under global warming scenarios (IPCC, 2022). Recent projections indicate that the country could experience temperature increases exceeding 2 °C by the mid-21st century, accompanied by a higher frequency of extreme climatic events, posing a direct threat to the stability and sustainability of mountain agricultural systems (United States Agency for International Development [USAID], 2017; World Bank, 2020).

Species distribution models (SDMs), particularly MaxEnt, have been widely applied to assess coffee climatic suitability under climate change scenarios across Africa, Asia, and Latin America (Chemura et al., 2021; Ovalle-Rivera et al., 2015; Zhang et al., 2022). The MaxEnt model, grounded in the principle of maximum entropy (Phillips et al., 2004), estimates species presence probability using occurrence-only records and has become a robust and widely adopted tool in potential distribution studies (Avalos et al., 2023; Fitzgibbon et al., 2022; Promnun et al., 2020). Numerous studies have demonstrated its effectiveness for evaluating *C. arabica* habitat suitability under climate change scenarios in Africa (Benti et al., 2022), Asia, (Purba et al., 2019; Zhang et al., 2022), and Latin America (Chalchissa et al., 2022; García et al., 2018). These studies consistently identify key determinants such as annual precipitation, mean temperature, altitude, slope, and soil type, and report an upslope shift of suitable areas under warming scenarios particularly under the Representative Concentration Pathway 4.5 (RCP4.5) and RCP8.5. Additionally, several authors have applied MaxEnt with climatic predictors to model coffee land suitability across diverse geographical contexts (Burbano-Cushica and Flores-Chiriboga, 2022; Cassamo et al., 2023; Chemura et al., 2021; Fain et al., 2018; García et al., 2018; Lara-Estrada et al., 2021; Rabelo de Oliveira et al., 2018; Zhang et al., 2021).

Nevertheless, relevant knowledge gaps persist for the Peruvian context. Existing assessments in the country have largely focused on regional or subnational scales, such as agroecological suitability studies in the Amazonas region based on multicriteria GIS approaches (Salas et al., 2020), or more recent territorial zoning initiatives developed for Cajamarca (Gómez-Fernández et al., 2025). While these studies represent valuable contributions to regional planning, they do not comprehensively address the national-scale spatial reconfiguration of coffee agroclimatic suitability, nor do they explicitly quantify the direction and magnitude of suitability shifts under multiple SSP scenarios and temporal horizons.

Moreover, the current context of increasing sustainability and traceability requirements in international markets has highlighted the need to identify agriculturally suitable territories outside forested areas, particularly for commodities associated with deforestation risk, such as coffee (European Commission, 2024; 2025; Pendrill et al., 2019). In this framework, recent regulations promoting deforestation-free supply chains further underscore the importance of integrating biophysical suitability assessments with land-use planning criteria (European Commission, 2023).

In this study, we modeled the potential distribution of *C. arabica* in Peru under current and future climatic conditions using the MaxEnt algorithm, integrating climatic, topographic, and edaphic variables. Agroclimatic suitability was evaluated under Shared Socioeconomic Pathway 1–2.6 (SSP1–2.6), SSP2–4.5, SSP3–7.0, and SSP5–8.5 scenarios for the temporal horizons of 2050, 2070, and 2090, and the direction and magnitude of spatial suitability shifts were analyzed. In doing so, this study contributes to filling a critical gap in the Peruvian literature by providing a national-scale, multiscenario, and spatially explicit assessment that can serve as a scientific basis for land-use planning, public policy design, and the development of climate adaptation strategies for the coffee sector.

2 Materials y methods

2.1 Study area

The study was conducted in the Republic of Peru, located in western South America between latitudes 0°01′48″S and 18°21′03″S

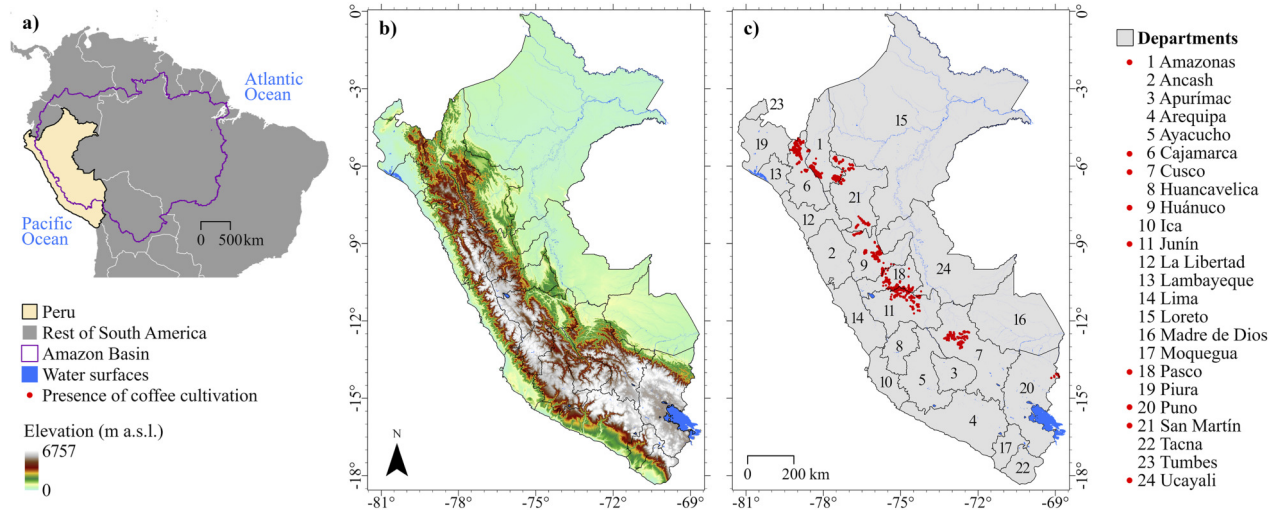

FIGURE 1
Spatial pattern of coffea arabica presence across the study area. **(a)** Geographic location of Peru within South America and the Amazon Basin. **(b)** Topographic map of Peru showing elevation gradients (m a.s.l.) and **(c)** Distribution of coffea arabica presence records across the 24 departments of Peru.

and longitudes 68°39′27″W and 81°20′13″W (Figure 1a). Peru covers approximately 1,285,216 km^2 and exhibits pronounced topographic and climatic heterogeneity, typically described across three major physiographic regions: the coast (flat and arid), the highlands (Andean, steep relief), and the rainforest (Amazonian and humid) (Figure 1b). This physiographic structure generates a wide range of microclimates and confers high agroecological variability that supports diverse cropping systems, including coffee.

Coffee cultivation in Peru is concentrated mainly on the eastern slopes of the Andes within the "ceja de selva" transition zone, generally between 800 and 2,200 m a.s.l., where agroclimatic conditions are favorable for crop establishment and production. The principal producing regions include Cajamarca, Amazonas, San Martín, Junín, and Pasco (Figure 1c), which together contribute more than 70% of national production (Ministerio de Desarrollo Agrario y Reigo [MIDAGRI], 2023). These areas are commonly characterized by acidic, well-drained soils, mean annual temperatures of approximately 18 °C–24 °C, and annual precipitation ranging from 1,200 to 2,500 mm (Servicio Nacional de Meteorología e Hidrología [SENAMHI], 2022), —critical factors in determining crop suitability (Abdelwahab et al., 2024). Such climatic and edaphic conditions are widely recognized as key determinants of coffee suitability and performance.

Selecting Peru as a case study provides a strategic setting for assessing climate change implications for globally important crops in tropical mountain systems, where strong altitudinal gradients, terrain fragmentation, and microclimatic variability can shape both exposure and adaptive capacity of agroproductive landscapes.

To simulate the spatial distribution of *C. arabica* in Peru under current and future climate conditions, we developed a modeling framework based on the systematic acquisition, standardization, and processing of environmental predictors, including bioclimatic, topographic, and edaphic variables. Georeferenced occurrence records of *C. arabica* were compiled and used as primary inputs for model development. The methodological workflow consisted of three main steps: (i) collection and filtering of presence records, together with the preparation of environmental layers required for implementation of the MaxEnt algorithm; (ii) model calibration through multiple parameter configurations, with the relative contribution of each predictor evaluated using a jackknife test to optimize model performance; and (iii) model validation using 25% of the occurrence records as an independent test dataset, with model accuracy assessed using the Area Under the Curve (AUC). Future habitat suitability was projected to the year 2100 using the MIROC6 general circulation model under different climate change scenarios defined by the SSPs.

2.2 Coffee presence data sources

Data on the spatial distribution of coffee (*C. arabica*) in Peru were compiled from multiple sources (Figure 1c). Georeferenced occurrence records were obtained from the Global Biodiversity Information Facility (GBIF; https://www.gbif.org/) using the GBIF AppEARs plugin in QGIS 3.28 (Ortega et al., 2017; Rojas-Briceño et al., 2022), and complemented with citizen science observations from the iNaturalist platform (https://www.inaturalist.org) (Li et al., 2024). Additional records were retrieved from the geospatial viewer developed under the European Union Deforestation-Free Products Regulation (EUDR) for Peru (https://ee-geomatica101.projects.earthengine.app/view/moduloavanceeu), implemented by the Ministry of Agrarian Development and Irrigation (MIDAGRI). Occurrence records lacking precise geographic coordinates were manually georeferenced using high-resolution satellite imagery in Google Earth.

A proprietary database was also assembled, incorporating field-collected presence records obtained using GPS devices, data provided by coffee-producing agricultural cooperatives, and records extracted from relevant peer-reviewed studies

TABLE 1 Climatic variables used in the MaxEnt model.

Category	Variable	Symbol	Units
Bioclimatic	Annual mean temperature	bio01	°C
	Mean diurnal range	bio02	
	Isothermality (Bio2/Bio7) (* 100)	bio03	Dimensionless
	Temperature seasonality (standard deviation *100)	bio04	
	Max. temperature of the warmest month	bio05	°C
	Min. temperature of coldest month	bio06	
	Temperature annual range (Bio5-Bio6)	bio07	
	Mean temperature of wettest quarter	bio08	
	Mean temperature of driest quarter	bio09	
	Mean temperature of warmest quarter	bio10	
	Mean temperature of coldest quarter	bio11	
	Annual precipitation	bio12	mm
	Precipitation of wettest month	bio13	
	Precipitation of driest month	bio14	
	Precipitation seasonality	bio15	Dimensionless
	Precipitation of wettest quarter	bio16	mm
	Precipitation of driest quarter	bio17	
	Precipitation of warmest quarter	bio18	
	Precipitation of coldest quarter	bio19	
Topographic	Elevation above mean sea level	Altitude	m a.s.l
	Terrain slope	Slope	°
	Terrain aspect	Aspect	
Edaphic	Topsoil sand fraction	Sand	%
	Topsoil silt fraction	Silt	
	Topsoil clay fraction	Clay	
	Organic carbon content	soc	g/kg
	pH value (H_2O)	phh2o	pH units
	Total nitrogen content	Nitrogen	g/kg
	The bulk density (bdod) of the fine earth fraction of the soil	bdod	kg/dm^3
	Volumetric fraction of coarse fragments	cfvo	% (vol.)

(Haro et al., 2025; Salas et al., 2020; Wigoberto Alvarado et al., 2022). In total, 16,364 georeferenced records were compiled, each including geographic coordinates (latitude and longitude) and the scientific name of the species (Gong et al., 2022).

To reduce spatial autocorrelation and minimize sampling bias in environmental suitability modeling, a systematic data-cleaning procedure was applied (Zhang et al., 2022). Duplicate records were removed, and only one occurrence point was retained per 250-m grid cell, corresponding to the spatial resolution of the environmental predictors. After spatial filtering, the final dataset consisted of 4,584 unique *C. arabica* presence records.

2.3 Environmental data (climate, soil, and topography)

The distribution and growth of plant species are strongly influenced by environmental factors, particularly climate, soil, and topography (Barboza et al., 2024; Yang et al., 2022). To account for these drivers, we selected a total of 30 environmental predictors (Table 1). Nineteen bioclimatic variables representing baseline climatic conditions for the period 1970–2000 were obtained from the WorldClim version 2.1 dataset at a spatial resolution of approximately 1 km (30 arc-seconds) and processed using Google

Earth Engine (GEE) (Fick and Hijmans, 2017). Topographic variables, including elevation, slope, and aspect, were derived from a Digital Elevation Model (DEM) provided by the CGIAR Consortium for Spatial Information (SRTM) (Farr et al., 2007; Rojas-Briceño et al., 2022). Soil properties were represented by eight variables obtained from the SoilGrids v0.5.3 database at a spatial resolution of 250 m and processed in GEE (Poggio et al., 2021). All environmental layers were subsequently standardized in ArcGIS 10.8, resampled to a uniform 250-m spatial resolution, and exported in ASCII format for use in species distribution modeling.

2.4 Future climate change scenarios

Future climate scenarios were derived from the Scenario Model Intercomparison Project (ScenarioMIP) within Phase 6 of the Coupled Model Intercomparison Project (CMIP6) (Chaulagain et al., 2025; O'Neill et al., 2016). This framework integrates anthropogenic emission trajectories with alternative socioeconomic development SSP–RCP approach (Eyring et al., 2016; Jones et al., 2016).

Specifically, SSP1–2.6 represents a sustainability-oriented pathway that limits global warming to below 1.5 °C by 2100, whereas SSP2–4.5 reflects an intermediate stabilization pathway with radiative forcing reaching 4.5 W m^{-2} (watts per square meter) by the end of the century, defined as the change in the Earth's energy balance per unit area due to greenhouse gases and other radiative forcing agents relative to preindustrial conditions. SSP3–7.0 combines high societal vulnerability with strong anthropogenic forcing (Zhang et al., 2022), while SSP5–8.5 represents the most extreme development pathway, resulting in radiative forcing of 8.5 W m^{-2} by 2100 (O'Neill et al., 2016; Zhang et al., 2021).

In this study, future projections were obtained from the Model for Interdisciplinary Research on Climate version 6 (MIROC6), using bioclimatic averages for the four scenarios (SSP1–2.6, SSP2–4.5, SSP3–7.0, and SSP5–8.5) (O'Neill et al., 2016). Climate datasets were retrieved from WorldClim for three future 20-year periods (2041–2060, 2061–2080, and 2081–2100) (https://www.worldclim.org/data/cmip6/cmip6climate.html) (Cárdenas et al., 2023). All future climate layers were processed using the same workflow applied to current conditions, ensuring consistency in spatial resolution and temporal comparisons.

2.5 Selection and processing of predictor variables

Prior to implementing the MaxEnt model, a rigorous selection and cleaning procedure was applied to the environmental variables to reduce multicollinearity, redundancy, and spatial autocorrelation, which can lead to model overfitting and reduced predictive performance (Adane, 2024; Booth, 2018; Li et al., 2024; Liu et al., 2025).

First, to minimize multicollinearity and ensure statistical independence among predictors, a Pearson correlation analysis was conducted across the full set of environmental variables in R, using both a correlation matrix and hierarchical clustering (dendrogram). An exclusion threshold of $|r| \geq 0.80$ was applied, and within each group of highly correlated variables, only the predictor with the greatest ecological relevance for coffee cultivation was retained (Dormann et al., 2013; González-Orozco et al., 2024; Zhang et al., 2022).

The retained variables were subsequently evaluated using a preliminary MaxEnt model (see Section 2.6 for details). Predictors showing negligible or null contributions to model performance were excluded, resulting in an optimized set of environmental variables (Avalos et al., 2023; Gomes et al., 2020). This two-step approach—combining correlation-based filtering with preliminary model evaluation—ensured the selection of ecologically meaningful and statistically non-redundant predictors, thereby improving the robustness and reliability of the final model. All analyses were conducted in RStudio version 4.2.1 (R Core Team, 2020).

2.6 Species distribution modeling using MaxEnt

MaxEnt is widely recognized as one of the most robust methods for species distribution modeling when only presence data are available, particularly when using herbarium records or biological collection data (Brummitt et al., 2021; Li et al., 2023). By characterizing the environmental conditions associated with known occurrences of a target species, the model estimates relative habitat suitability as a continuous surface, based on predictors such as temperature and precipitation, and projects these conditions spatially to identify areas that meet the species' ecological requirements (Chen et al., 2024).

To estimate the potential distribution of *C. arabica*, we applied the MaxEnt algorithm (version 3.4.3) (Phillips et al., 2006). This correlative modeling approach quantifies statistical relationships between species occurrence records and environmental predictors by maximizing entropy subject to environmental constraints derived from the presence data. Model estimation is based on the principle of maximum entropy, which aims to derive the probability distribution that maximizes entropy under environmental constraints, as defined in Equation 1

$$H(p) = \sum_{x \in X} p(x) \ln p(x) \quad (1)$$

where $p(x)$ represents the probability of species presence within a given environmental cell, and ln denotes the natural logarithm (Phillips et al., 2006).

Georeferenced occurrence records and environmental predictors—including bioclimatic, edaphic, and topographic variables—were integrated to generate logistic habitat suitability maps, with values ranging from 0 (unsuitable) to 1 (highly suitable). The MaxEnt model was run using 10,000 background points, a maximum of 5,000 iterations, and a convergence threshold of 1×10^{-5}, following parameter settings that are widely applied and validated in previous species distribution modeling studies (Phillips et al., 2006; 2017; Yang et al., 2022).

In contrast to a strictly default implementation, the modeling framework explicitly incorporated the hinge and threshold feature classes, which are recommended for datasets with a large number of presence records, as they allow the capture of complex non-linear relationships between the species and the environment while maintaining adequate control over model complexity (Merow et al., 2013; Phillips et al., 2017; Phillips and Miroslav, 2008).

A comprehensive exploration of regularization multipliers and all possible combinations of feature classes was not conducted; however, this configuration was considered appropriate given the quality and size of the dataset, as well as the prior procedures applied to control multicollinearity and spatial autocorrelation in occurrence records (Radosavljevic and Anderson, 2014; Shcheglovitova and Anderson, 2013).

Model performance was evaluated using an internal cross-validation approach, with 75% of the presence records used for model calibration and the remaining 25% reserved for validation—an evaluation scheme commonly applied in species distribution models when robust and spatially filtered datasets are available (Elith et al., 2011; Li et al., 2023; Muscarella et al., 2014; Wang et al., 2023). Predictive performance was assessed using the Area Under the Curve (AUC) of the Receiver Operating Characteristic (ROC) curve, adopting the following interpretation thresholds: AUC <0.6 (no predictive capacity), 0.6–0.7 (low), 0.7–0.8 (moderate), 0.8–0.9 (good), and >0.9 (excellent) (Sun et al., 2020; Wu et al., 2024). Ten replicate model runs were performed, and the model with the highest AUC value was selected as the final model (Li et al., 2024; Zhang et al., 2022).

The relative importance of predictor variables was assessed using the jackknife test, both individually and in combination, and complemented by estimates of percentage contribution and permutation importance—standard procedures implemented in MaxEnt to identify the influence of environmental predictors (Feng et al., 2019; Phillips et al., 2017). Model regularization was applied through the penalty structure associated with the selected feature classes, contributing to reduced overfitting and improved model generalization (Chen et al., 2024; Radosavljevic and Anderson, 2014). Finally, response curves were generated to evaluate the individual influence of each environmental variable on habitat suitability.

2.7 Classification of potential habitat

The MaxEnt results were transformed into raster format within ArcGIS Pro to enable spatial analyses. The resulting map of potential distribution depicted continuous suitability values between 0 and 1, indicating the relative environmental favorability for the species under study. To classify these areas, the natural breaks method was applied, segmenting the continuous gradient into discrete, ecologically interpretable classes.

Based on this reclassification, four habitat suitability categories were defined: unsuitable (<0.2), low suitability (0.2–0.4), moderate suitability (0.4–0.6), and high suitability (>0.6). This classification allowed clear differentiation between marginal regions and core potential cultivation zones for *C. arabica*.

2.8 Estimation of the current suitable area for coffee cultivation

To delineate areas with effective viability for the expansion of *C. arabica* in Peru, we applied a spatially explicit framework that integrated multiple exclusion criteria and prioritization rules. The analysis accounted for biophysical, legal, and deforestation-related constraints. This approach follows established frameworks for agricultural suitability assessment and land-use change analysis in tropical cropping systems (Cotrina-sanchez et al., 2026; Kamath et al., 2024).

In the case 1, ecosystems unsuitable for agricultural activities were excluded, including rivers, wetlands, mangroves, lakes and lagoons, glaciers, periglacial zones, coastal wetlands, artificial water bodies, urban areas, and mining zones (Figure 2a). These spatial layers were derived from Peru's national ecosystem map produced by the Ministry of the Environment (Ministerio del Ambiente, 2019a).

Case 2 incorporated legal restrictions by excluding areas under formal conservation status, including Protected Natural Areas (NA) and their buffer zones (ZA) designated by the National Service of Natural Protected Areas (Servicio Nacional de Áreas Naturales Protegidas por el Estado [SERNANP], 2025) (Figure 2b). PNA may be national, regional, or private, and may also be designated as permanent (definitive) or transitional. National PNA include the definitive categories National Parks (PN), National Sanctuaries (SN), Historic Sanctuaries (SH), Communal Reserves (RC), Protected Forests (BP), and others, as well as the transitional category Reserved Zones (ZR). Regional definitive PNA correspond to the category Regional Conservation Areas (ACR), whereas private PNA (definitive or transitional) correspond to the category Private Conservation Areas (ACP). Among national or regional definitive PNA categories, those classified as indirect-use (PN, SN, SH) prohibit resource extraction or environmental modification, while direct-use categories (RC, BP, ACR, and others) allow resource use under approved management plans (Rojas-Briceño et al., 2025; SERNANP, 2023).

In the case 3, forest-cover constraints were applied to ensure compliance with the European Union Regulation on deforestation-free products (EUDR), which requires that coffee exported to international markets originate from areas without deforestation after 2020 (European Commission, 2023). Forest-cover data were obtained from the Global Map of Forest Cover 2020 (version 2, Figure 2c), developed by the Joint Research Centre of the European Commission (Bourgoin et al., 2024).

Case 4 applies all restrictions from the previous cases, representing a fully constrained scenario that integrates biophysical (ecosystems unsuitable), legal, and deforestation-free criteria.

2.9 Identification of areas for productive restoration

Degraded lands with potential for productive restoration were identified, prioritizing their use as a dual strategy to reduce pressure on natural forest ecosystems while promoting a resilient and environmentally responsible coffee sector (UNEP and FAO, 2021). Degraded areas were identified using the national degraded lands map (2022) produced by Ministerio del Ambiente (2025), which has been widely applied in land restoration and suitability assessments (Coronel-castro et al., 2025; Cotrina et al., 2021; Rojas-Briceño et al., 2020). This dataset classifies land degradation into four main categories—non-degraded, low, medium, and high—based on indicators such as changes in vegetation cover, forest fragmentation, net primary productivity (NPP), and forest loss (Ministerio del Ambiente, 2019b). In this study, forest loss was updated for the period 2001–2024 using geospatial data from (Ministerio del Ambiente, 2026), which constitute the baseline source for the development of the degradation map (Ministerio del Ambiente, 2019a).

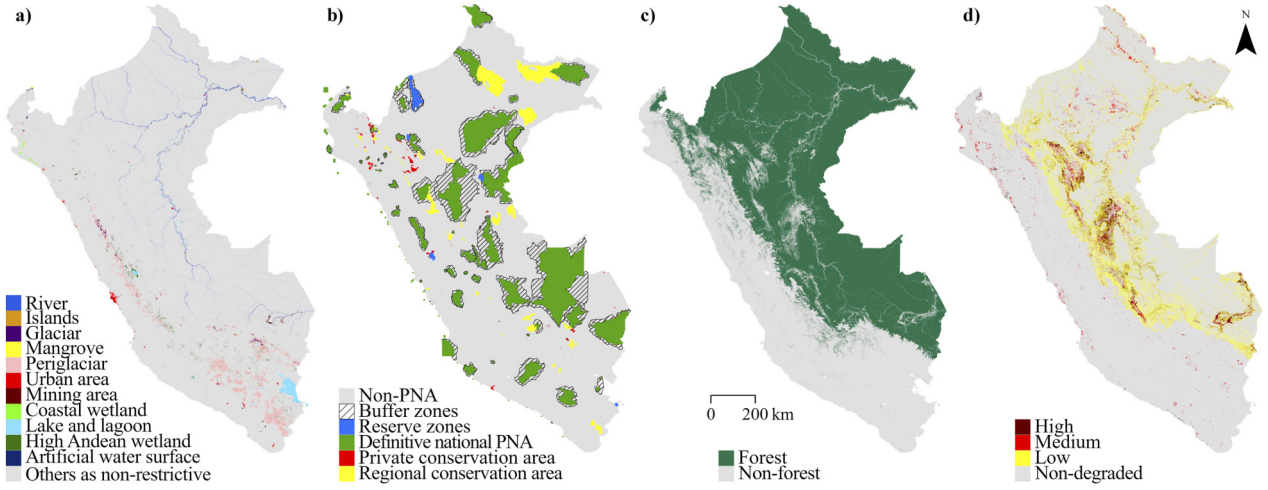

FIGURE 2
Spatial exclusion datasets, including degraded lands, used to estimate the current suitable area for coffee cultivation in Peru. **(a)** Ecosystems **(b)** PNA, Protected natural areas **(c)** Global map of forest cover 2020 **(d)** Degraded areas.

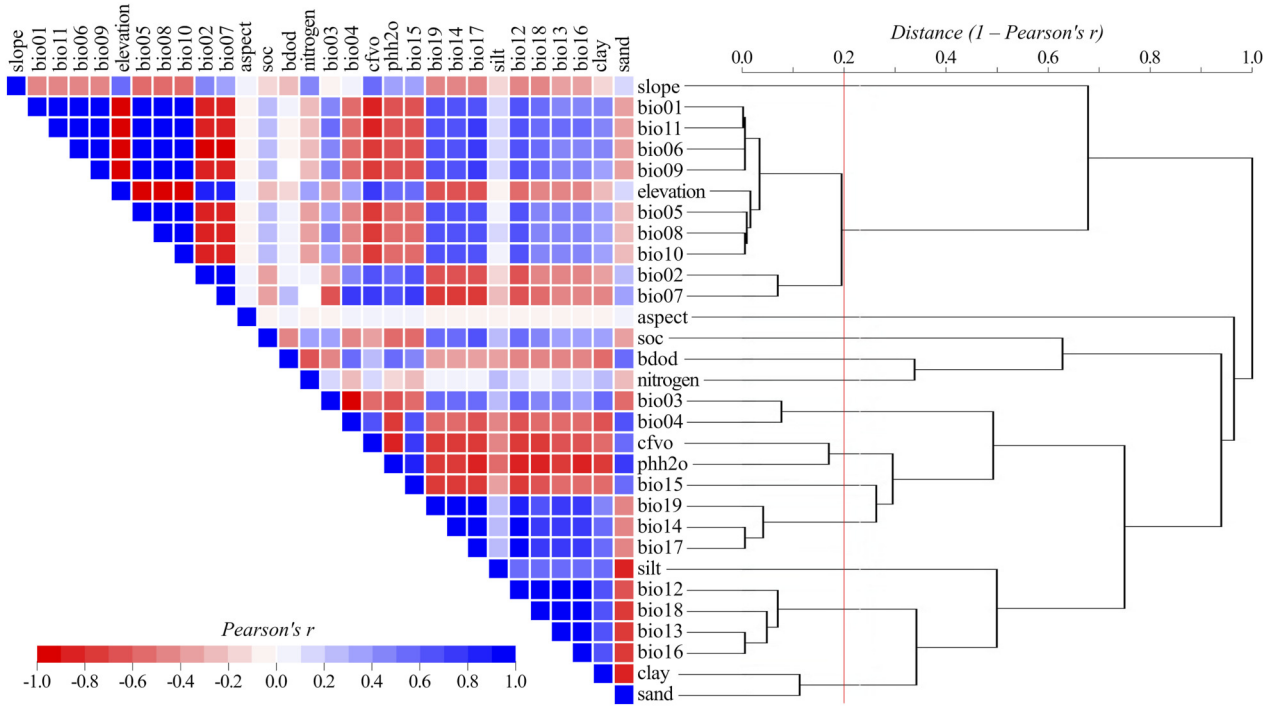

FIGURE 3
Pearson correlation matrix among the environmental variables and hierarchical clustering dendrogram of intercorrelated groups.

3 Results

3.1 Selection and clustering of environmental variables

The initial assessment of multicollinearity among environmental variables was visualized using a Pearson correlation matrix (Figure 3). The matrix revealed a structured pattern of both positive (blue) and negative (red) correlations, enabling the identification of clusters of highly correlated predictors. A prominent cluster was formed by temperature- and seasonality-related bioclimatic variables (bio01, bio05, bio06, bio08, bio09, bio10, bio11, and bio19), which exhibited strong positive correlations approaching unity, indicating a high degree of statistical

redundancy. Similarly, edaphic variables associated with soil texture (sand, silt, and clay) showed strong internal correlations, while topographic variables such as elevation and slope clustered along the same altitudinal gradient.

In contrast, other edaphic and soil chemical variables, including pH, soil organic carbon (soc), nitrogen, and bulk density (bdod), displayed more heterogeneous correlation patterns with the bioclimatic predictors, suggesting that they provide complementary and largely non-redundant information. This result underscores their relevance for subsequent modeling stages, as these variables capture environmental dimensions not fully represented by the highly collinear climatic and topographic predictors.

In addition, hierarchical clustering analysis further refined these relationships and is illustrated in the dendrogram shown in Figure 3, constructed using the distance metric 1−|r|1 - |r|1−|r| and a cutoff threshold of 0.8. This approach identified 13 distinct clusters of correlated variables, each comprising one or more predictors with strong internal associations. For subsequent modeling steps, a single representative variable was selected from each cluster, prioritizing ecological relevance and statistical independence.

This variable reduction strategy resulted in a robust set of environmental predictors while minimizing redundancy and reducing the risk of overfitting in ecological niche modeling. Overall, the combined interpretation of the correlation matrix and the hierarchical clustering dendrogram (Figure 3) provided a sound basis for objective predictor selection, ensuring model stability, interpretability, and generalization capacity.

3.2 MaxEnt model accuracy

Model accuracy was assessed using a combined evaluation of omission rates and the Area Under the Curve (AUC), both of which are widely used metrics for validating species distribution models. The omission rate analysis allows the detection of potential bias or overfitting by comparing the proportion of occurrence records incorrectly predicted as absent with the expected theoretical omission rate across different probability thresholds. When observed and predicted omission rates closely match, the model is considered well calibrated and not overfitted (Wu et al., 2024). Moreover, limited deviation of the omission curve from the theoretical expectation suggests low spatial autocorrelation in the occurrence data (Shcheglovitova and Anderson, 2013).

In this study, the omission curves derived from ten replicate model runs showed a high level of agreement between predicted and observed omission rates for the test data (Figure 4a), indicating appropriate model calibration and confirming the spatial independence of the occurrence records.

Model performance was further evaluated using the Receiver Operating Characteristic (ROC) curve generated by MaxEnt. Under current climatic conditions, the *C. arabica* distribution model yielded a mean AUC value of 0.858, with no variation among replicates (Figure 4b). According to commonly accepted thresholds, this value corresponds to a *good* level of predictive accuracy, demonstrating the model's ability to reliably discriminate between environmentally suitable and unsuitable areas and to perform substantially better than random predictions.

3.3 Contribution of environmental variables

The MaxEnt model results revealed that various environmental variables exert different levels of influence on the potential distribution of *C. arabica*. The Jackknife analysis of regularized training gain (Figure 4c) showed that altitude, precipitation of the driest quarter (bio17), soil nitrogen content, and soil pH in water (phh2o) were the most influential variables. These variables demonstrated high importance both when used in isolation and when omitted from the model, underscoring their essential role in predicting suitable habitat for the species.

The percentage contribution results (Figure 4d) confirmed the importance of bio17 and elevation, contributing 29.7% and 21.8%, respectively. These were followed by bulk density of the fine soil fraction (bdod) at 14.3%, isothermality (bio03) at 11.8%, and slope at 7.4%. The least influential variables were terrain aspect (0.2%), soil organic carbon (soc) (0.7%), and phh2o (0.9%).

The jackknife analysis performed under different future climate scenarios (Figure 5) revealed consistent patterns in the relative importance of key environmental variables. Across most scenarios, altitude, bio17, bio15 (precipitation seasonality), bio03, bulk density (bdod), and soil nitrogen content exhibited high training gains when used in isolation and a marked decrease in gain when omitted from the model. This pattern indicates that these variables make strong and independent contributions to model performance. Their sustained influence across scenarios suggests that they are robust determinants of the future distribution of *C. arabica*, underscoring their relevance for species distribution projections under uncertain climatic conditions.

MaxEnt response curves (Figures 4e–P) illustrated how the probability of presence of *C. arabica* varies with changes in the most influential variables. Altitude displayed a unimodal relationship, with maximum probability between 1,500 and 2,000 m a.s.l., declining outside this range (Figure 4j). Precipitation of the driest quarter (bio17) also showed a unimodal response, with an optimum near 200 mm (Figure 4i). Soil nitrogen content (Figure 4k) and soil pH in water (Figure 4l) displayed positive relationships, indicating greater habitat suitability with increased values within certain limits.

Other variables such as bio3 (Figure 4f) and bio15 (Figure 4h) exhibited more complex responses, whereas sand and silt content (Figures 4m,n) showed negative trends as their values increased. Slope (Figure 4o) presented a nonlinear relationship, suggesting that moderate slopes may be more suitable.

3.4 Potential distribution of coffee cultivation

Using the MaxEnt model, we estimated the current potential distribution of *C. arabica* across Peru's 24 administrative departments (Figure 6). Excluding biophysical barriers (Case 1; Figure 6a), at the national scale, areas classified as highly suitable accounted for 42,322.95 km^2 (3.3% of the national territory), moderately suitable areas covered 51,907.84 km^2 (4.0%), and low-suitability areas encompassed 59,784.95 km^2 (4.6%), whereas 88.0% of its territory was identified as unsuitable or restricted under current climatic conditions. The spatial footprint of suitable habitats is primarily concentrated along corridors on the eastern

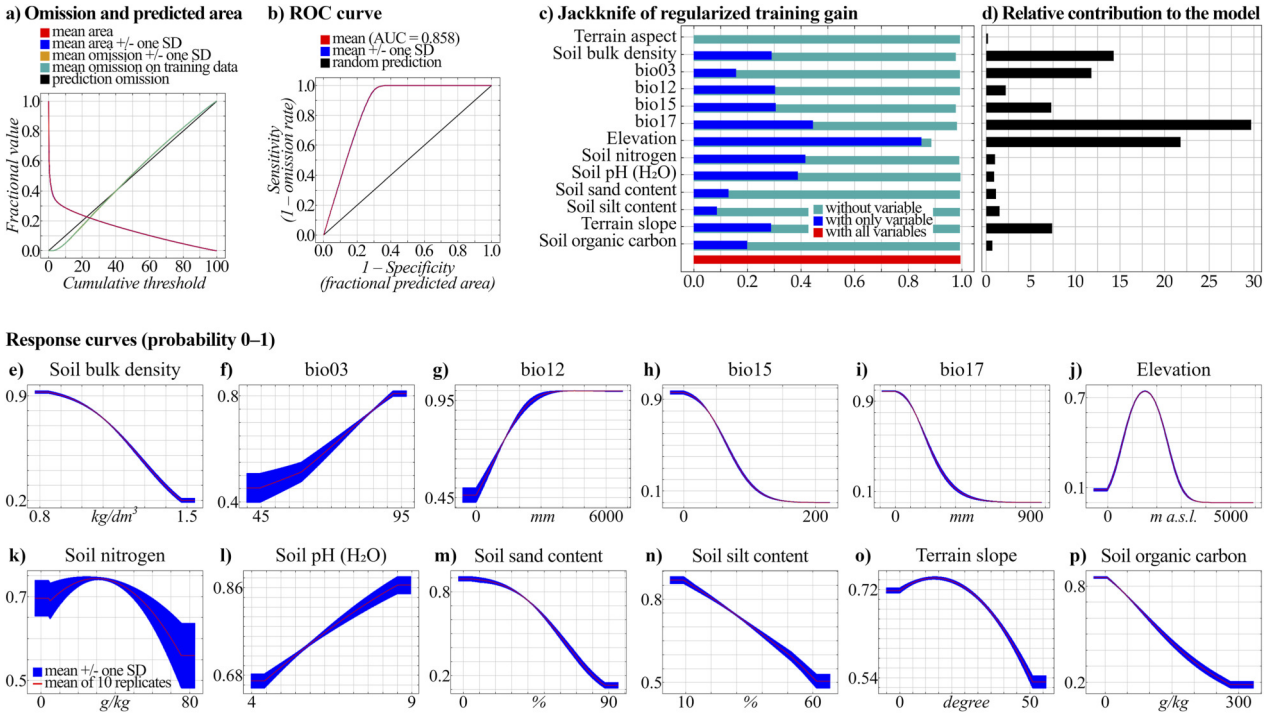

FIGURE 4
MaxEnt model accuracy based on omission rates **(a)** and receiver operating characteristic **(b)**, variable importance assessed by jackknife tests **(c)** and relative contributions **(d)**, and response curves of the main environmental variables **(e–p)** for *Coffea arabica* under current climatic conditions.

slopes of the Andes. When legally protected areas are also excluded (Case 2; Figure 6b), 62.5% (26,453.64 km^2), 59.4% (30,827.60 km^2), and 60.7% (36,290.48 km^2) of the high, moderate, and low suitability areas, respectively, identified under the base Case 1 are retained. In contrast, these proportions are sharply reduced to 11.7% (4,949.26 km^2), 15.3% (7,923.07 km^2), and 20.0% (11,973.59 km^2) when forest cover is excluded from Case 1 (Case 3; Figure 6c), and further decrease to 11.0% (4,666.09 km^2), 13.8% (7,154.93 km^2), and 18.2% (10,870.58 km^2) when both protected areas and forest cover are excluded (Case 4; Figure 6d).

The department-level breakdown (Figure 6e) sharpens the pattern shown in Figure 6a and confirms that high suitability is concentrated along the central–northeastern Andean–Amazonian gradient. San Martín leads with 9,304.06 km^2 (18.2% of its territory) in the high class and 9,990.06 km^2 (19.6%) in the moderate class, followed by Cusco (6,287.08 km^2 [8.7%] and 6,779.65 km^2 [9.4%]), Junín (5,515.38 km^2 [12.5%] and 6,560.20 km^2 [14.8%]), and Cajamarca (5,098.26 km^2 [15.5%] and 5,614.33 km^2 [17.0%]). Amazonas (4,434.29 km^2, 11.3% of its territory), Huánuco (3,682.52 km^2, 9.8%), and Pasco (3,666.71 km^2, 15.4%) are also noteworthy with high suitability areas. In contrast, several coastal and far-southern departments record zero area in the high class—Arequipa, Ica, Lambayeque, Lima, Tacna, and Tumbes—whereas Ancash (35.66 km^2), Huancavelica (52.67 km^2), Piura (98.09 km^2), and Puno (17.81 km^2) show residual values, reflecting temperature–moisture and edaphic constraints. In the lowland Amazon, Loreto (423.26 km^2) and Madre de Dios (792.17 km^2) illustrate a reduced area classified as highly suitable, suggesting that optimal conditions are confined to very specific elevational enclaves.

When protected areas are also excluded (Case 2, Figure 6b), the extent of highly suitable land decreases but remains substantial in Cajamarca (4,883.49 km^2, 14.8% of its territory), San Martín (4,607.89 km^2, 9.0%), Amazonas (3,832.60 km^2, 9.7%), Junín (3,585.22 km^2, 8.1%), and Cusco (3,476.88 km^2, 4.8%) (Figure 6f), thereby preserving the central–northeastern Andean–Amazonian gradient. The additional exclusion of forest cover (Case 3, Figure 6c) results in a pronounced contraction of suitable areas: only Cajamarca (2,075.91 km^2, 6.3% of its territory) and Amazonas (1,258.35 km^2, 3.2%) retain more than 1,000 km^2 of highly suitable land, while most departments fall below 290 km^2 (Figure 6g). Finally, the joint exclusion of protected areas and forest cover (Case 4, Figure 6d) maintains the pattern observed in Case 3, with a marginal additional reduction in highly suitable land (maximum difference ~65 km^2 relative to Case 3), leaving Cajamarca (2,011.00 km^2) and Amazonas (1,213.50 km^2) as the only departments remaining marginally prominent, while most departments fall below 275 km^2 (Figure 6h).

The retention percentages relative to the baseline case (Case 1), synthesize the territorial response to legal and land-cover constraints. Following the exclusion of protected areas (Case 2), only three (Pasco, Madre de Dios, and Loreto) out of the 16 departments that initially contained areas of high suitability failed to retain more than 50% of such areas (Figure 6f relative to Figure 6e). Among the seven departments with more than 3,600 km^2 of highly suitable land, Cajamarca stands out by maintaining 95.8% of its baseline extent; five departments retained between 50% (e.g., San Martín) and 87% (e.g., Amazonas), whereas Pasco retained only 22.5%. Ucayali, which

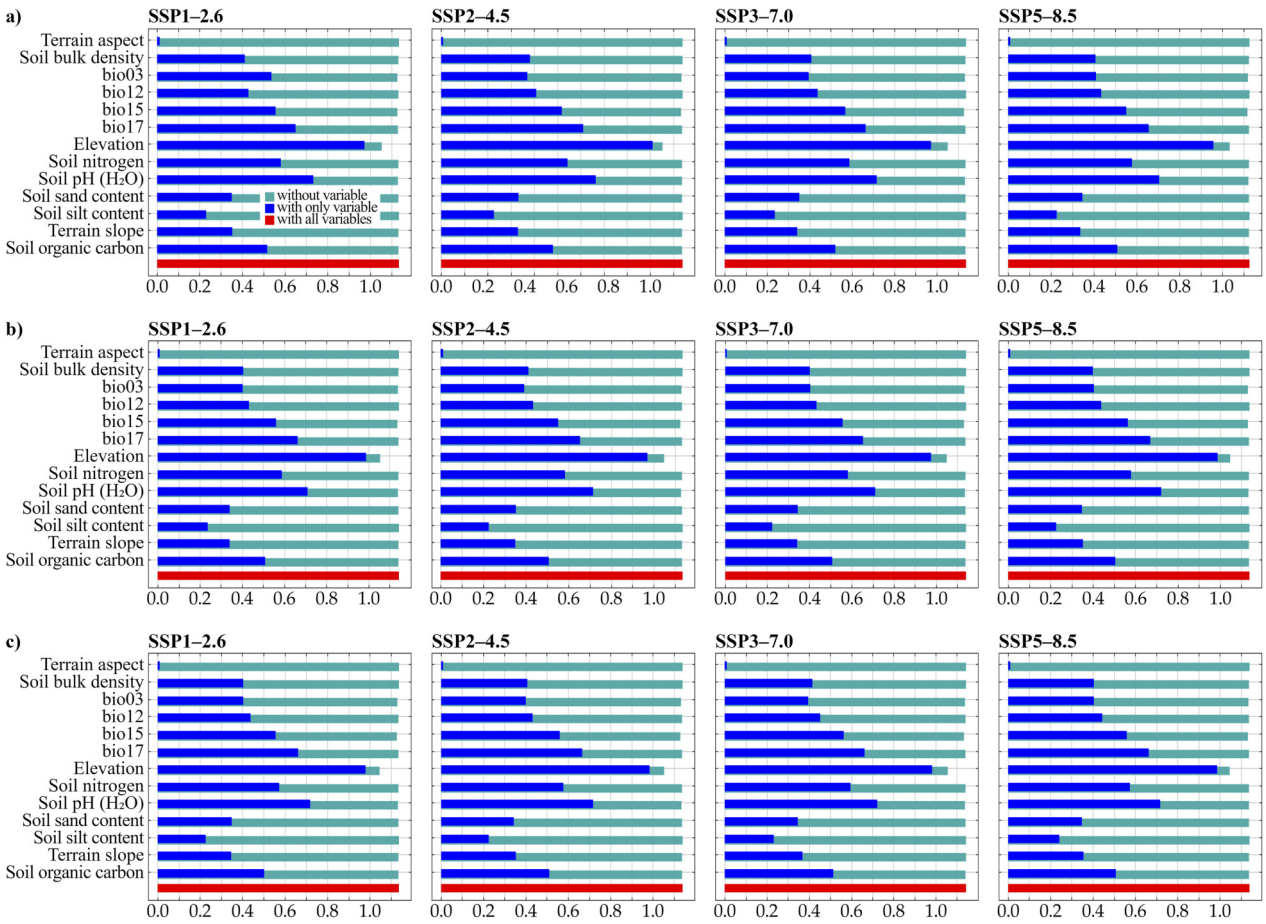

FIGURE 5
Jackknife test of regularized training gain in MaxEnt models across climate change scenarios, illustrating the relative contribution of environmental predictors to the projected future distribution of *Coffea arabica*. **(a)** 20250 **(b)** 2070 **(c)** 2090.

initially had ~1,600 km^2 of highly suitable land, showed a substantial retention of 73%. In contrast, among the eight departments with less than 850 km^2 of highly suitable area, La Libertad retained 74.3%, five departments retained between 94% and 100%, and the two Amazonian lowland departments (Loreto and Madre de Dios) experienced an almost complete collapse.

With the additional exclusion of forest cover (Case 3), retention declines sharply across most departments (Figure 6g relative to Figure 6e): 14 of the 16 departments that initially contained highly suitable areas retain less than 41% of their baseline extent, indicating high sensitivity to forest-cover constraints. Among the seven departments with more than 3,600 km^2 of highly suitable land, Cajamarca and Amazonas retain 40.7% and 28.4%, respectively, whereas the remaining five retain less than 5.5%. Ucayali, which initially had ~1,600 km^2 of highly suitable land, shows minimal retention of less than 2%. In contrast, among the eight departments with less than 850 km^2 of highly suitable area, Ancash retains 93.6%, La Libertad retains 51.2%, three departments retain between 20% and 38%, Puno retains 9%, and the two Amazonian lowland departments (Loreto and Madre de Dios) experience an almost complete collapse.

With the combined exclusion of protected areas and forest cover (Case 4), retention relative to Case 3 decreases by less than 1.3 percentage points in almost all departments (e.g., Cajamarca from 40.7% to 39.4%), with La Libertad as the only exception, where retention declines by 9.9 percentage points (Figure 6h relative to Figure 6e). This confirms that forest cover is the primary restrictive factor compared with currently established protected areas in Peru.

3.5 Protected natural areas at potential risk

Approximately 39% (16,502.88 km^2) of the areas classified as highly suitable for coffee cultivation overlap with 60 Protected Natural Areas (PNA) and 24 buffer zones (ZA), indicating potential spatial pressure associated with the expansion of coffee-based agroforestry systems. By PNA level, 64.24 km^2 correspond to two nationally administered transitional Reserved Zones (ZR), 184.95 km^2 to 21 permanent or transitional Private Conservation Areas (ACP), 1,003.34 km^2 to 16 permanent Regional Conservation Areas (ACR), 8,984.87 km^2 to 21 nationally administered permanent PNA (including five PNA categories), 6,261.42 km^2 to 23 ZA associated with these national PNA, and 4.05 km^2 to the ZA of ZR Chancaybaños (Figure 7). Among the 60 PNA, 26 contain areas of high suitability smaller than 10 km^2, 20 range between 10 and 100 km^2, six between 100 and 500 km^2, six between 500 and 1,000 km^2, and two exhibit the largest extents, corresponding to

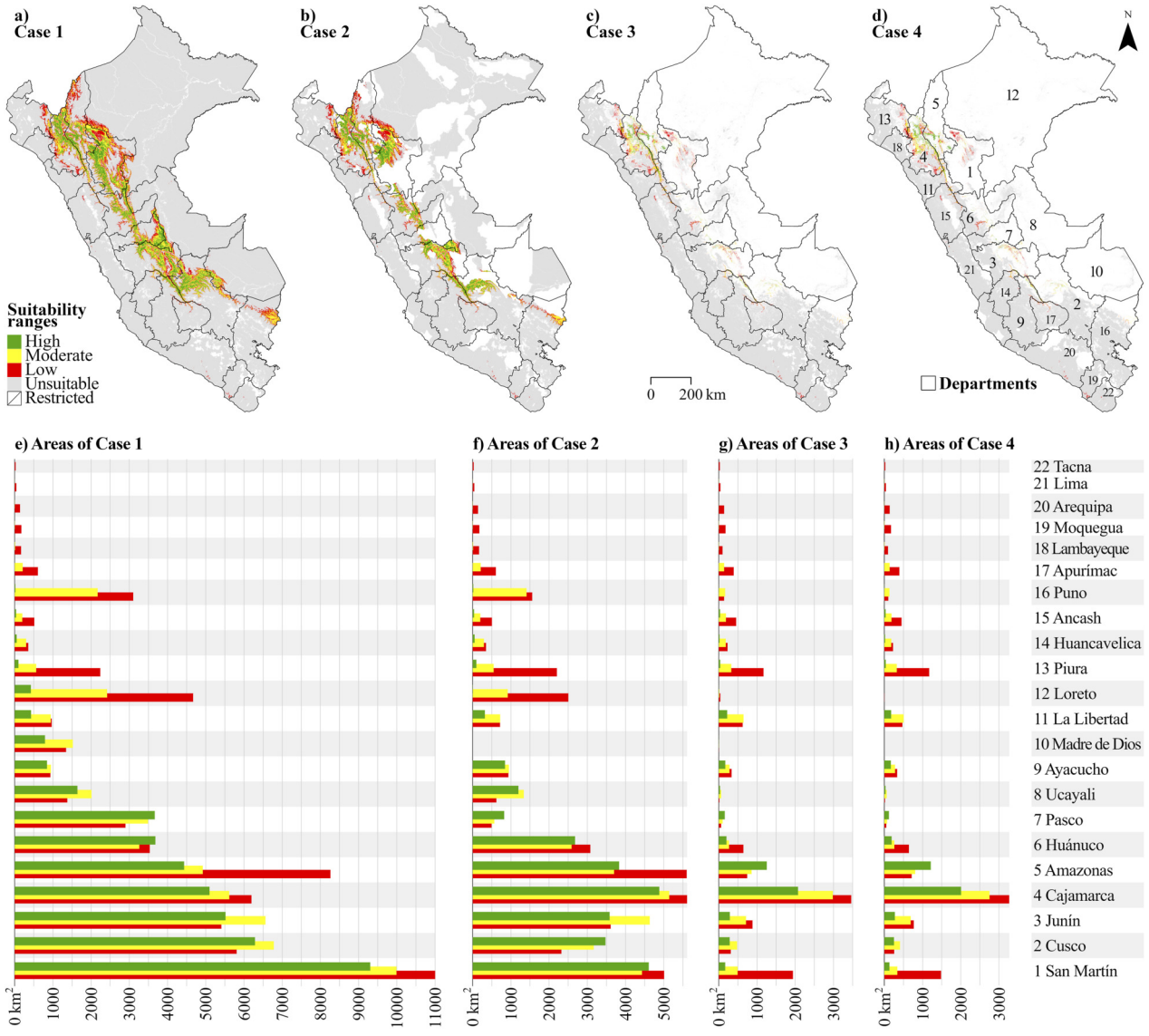

FIGURE 6
Spatial distribution of areas suitable for coffee cultivation under four exclusion cases: **(a)** biophysical barriers excluded (Case 1); **(b)** Case 1 plus exclusion of protected areas (Case 2); **(c)** Case 1 plus exclusion of forest cover (Case 3); **(d)** Case 1 plus exclusion of both protected areas and forest cover (Case 4); and **(e–h)** departmental suitable areas ordered by suitable-area extent.

RC El Sira (1,993.27 km^2) and PN Cordillera Azul (1,950.96 km^2). In contrast, among the 24 ZA, five contain areas of high suitability smaller than 10 km^2, nine range between 10 and 100 km^2, five between 100 and 500 km^2, four between 500 and 1,000 km^2, and the ZA of PN Río Abiseo exhibits the largest extent, at 1,732.65 km^2. Overall, areas of high suitability are greater within indirect-use PNA (5,018.63 km^2) than within direct-use PNA (4,969.59 km^2), and substantially greater than those within non-classified PNA (249.19 km^2).

3.6 Areas with restoration potential through coffee cultivation

Approximately 39.8% (16,852.33 km^2) of the areas classified as highly suitable for coffee cultivation overlap with low (30.5%, 12,918.64 km^2), medium (2.6%, 1,090.78 km^2), and high (6.7%, 2,842.91 km^2) degradation categories, the latter representing the area of greatest interest for productive restoration through coffee-based agroforestry systems (Figures 8a,b). Regarding areas classified as moderately suitable for coffee cultivation, 2.9% (1,522.21 km^2) and 5.9% (3,060.11 km^2) spatially overlap with medium and high degradation, respectively, and are likewise relevant for restoration. At the departmental level (Figure 8c), San Martín (716.97 km^2) and Junín (532.42 km^2) present the largest extents of high suitability intersecting with high degradation; seven departments range between 113.23 km^2 (e.g., Ayacucho) and 357.12 km^2 (e.g., Huánuco), and seven others between 0.11 km^2 (e.g., Ancash) and 8.97 km^2 (e.g., La Libertad). Similarly, San Martín (999.87 km^2) and Junín (731.26 km^2) also stand out in moderately suitable areas

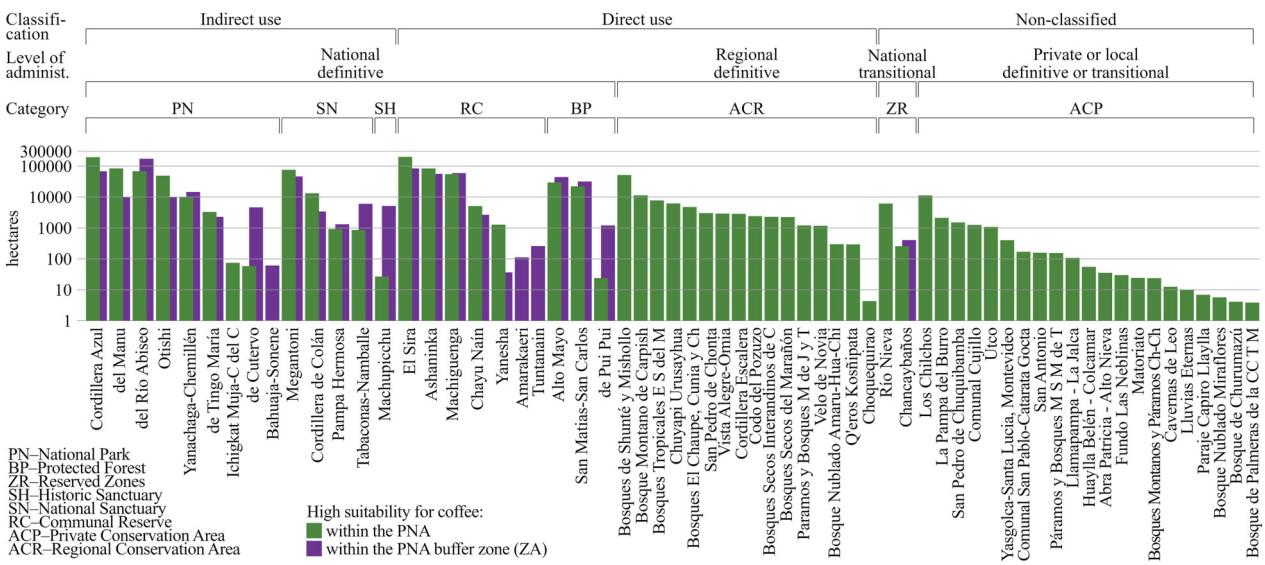

FIGURE 7
Area of high suitability for coffee within protected natural areas and their buffer zones.

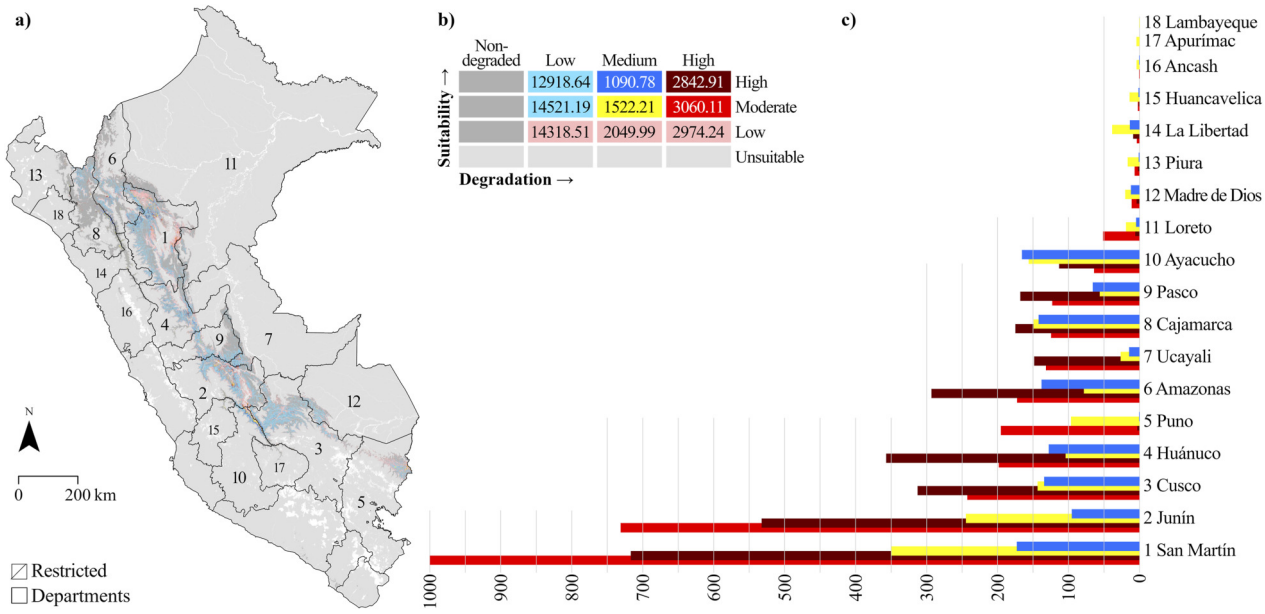

FIGURE 8
Degraded lands with potential for ecological restoration through coffee cultivation, showing their spatial distribution, aggregated area totals, and departmental areas. **(a)** Case 1 **(b)** Map legend and areas (km²) **(c)** Areas by department (km²).

intersecting with high degradation; seven departments range between 123.04 km² (e.g., Pasco) and 242.71 km² (e.g., Cusco), three between 11 and 64 km², and six below 7 km². For areas classified as high suitability intersecting with medium degradation, although overall surfaces are smaller, San Martín (172.87 km²) and Ayacucho (165.63 km²) stand out; four departments range between 127 and 143 km², five between 12 and 95 km², and five below 5 km².

3.7 Future climate–driven changes in the potential distribution of coffee

Relative to current conditions (1970–2000), high suitability areas decline consistently across all future periods and SSP scenarios, with reductions ranging from −23.38% to −41.72% in the 2050s, −34.95% to −38.67% in the 2070s, and −35.10% to −40.29% by the 2090s (Table 2). Moderately suitable areas exhibit smaller relative declines,

TABLE 2 Projected potential habitat area for *Coffea arabica* under future climate scenarios in Peru, relative change from current conditions (Δ%), proportion of suitable area (% of suitable), and share of national territory (% of Peru), by agroclimatic suitability class.

Climate scenario		Suitable						Unsuitable	
		High		Moderate		Low			
		km² (Δ% vs. current)	% of suitable [% of Peru]	km² (Δ% vs. current)	% of suitable [% of Peru]	km² (Δ% vs. current)	% of suitable [% of Peru]	km² (Δ% vs. current)	% of Peru
Current (1970–2000)		42,322.95	27.48 [3.28]	51,907.84	33.70 [4.03]	59,784.95	38.82 [4.64]	1,069,923.39	83.04
2041–2060 (2050s)	SSP1–2.6	25,919.95 (−38.76)	25.70 [2.01]	41,431.28 (−20.18)	41.08 [3.22]	33,493.91 (−43.98)	33.21 [2.60]	1,123,094.00 (+4.97)	87.16
	SSP2–4.5	32,428.36 (−23.38)	30.14 [2.52]	45,813.78 (−11.74)	42.58 [3.56]	29,346.13 (−50.91)	27.28 [2.28]	1,116,350.87 (+4.34)	86.64
	SSP3–7.0	26,217.60 (−38.05)	25.74 [2.03]	42,253.48 (−18.60)	41.49 [3.28]	33,365.23 (−44.19)	32.76 [2.59]	1,122,102.82 (+4.88)	87.09
	SSP5–8.5	24,665.53 (−41.72)	24.55 [1.91]	45,253.99 (−12.82)	45.03 [3.51]	30,570.82 (−48.87)	30.42 [2.37]	1,123,448.80 (+5.00)	87.19
2061–2080 (2070s)	SSP1–2.6	26,148.11 (−38.22)	25.27 [2.03]	46,786.75 (−9.87)	45.22 [3.63]	30,526.97 (−48.94)	29.51 [2.37]	1,120,477.31 (+4.73)	86.96
	SSP2–4.5	27,531.60 (−34.95)	26.96 [2.14]	43,141.49 (−16.89)	42.25 [3.35]	31,436.73 (−47.42)	30.79 [2.44]	1,121,829.31 (+4.85)	87.07
	SSP3–7.0	25,954.70 (−38.67)	25.88 [2.01]	43,906.96 (−15.41)	43.78 [3.41]	30,425.66 (−49.11)	30.34 [2.36]	1,123,651.81 (+5.02)	87.21
	SSP5–8.5	26,334.50 (−37.78)	25.77 [2.04]	42,841.88 (−17.47)	41.92 [3.32]	33,015.15 (−44.78)	32.31 [2.56]	1,121,747.61 (+4.84)	87.06
2081–2100 (2090s)	SSP1–2.6	27,466.01 (−35.10)	27.31 [2.13]	42,269.55 (−18.57)	42.03 [3.28]	30,824.58 (−48.44)	30.65 [2.39]	1,123,379.00 (+5.00)	87.19
	SSP2–4.5	25,348.02 (−40.11)	24.88 [1.97]	45,281.80 (−12.77)	44.44 [3.51]	31,258.79 (−47.71)	30.68 [2.43]	1,122,050.52 (+4.87)	87.08
	SSP3–7.0	25,271.58 (−40.29)	24.73 [1.96]	46,294.68 (−10.81)	45.29 [3.59]	30,643.18 (−48.74)	29.98 [2.38]	1,121,729.69 (+4.84)	87.06
	SSP5–8.5	25,904.24 (−38.79)	25.50 [2.01]	45,795.67 (−11.78)	45.08 [3.55]	29,891.05 (−50.00)	29.42 [2.32]	1,122,348.17 (+4.90)	87.11

ranging from −11.74% to −20.18% in the 2050s, −9.87% to −17.47% in the 2070s, and −10.81% to −18.57% in the 2090s, indicating comparatively greater resilience under projected climate change. Low suitability areas experience the strongest contractions, with reductions between −43.98% and −50.91% in the 2050s, −44.78% and −49.11% in the 2070s, and −47.71% and −50.00% in the 2090s. In contrast, unsuitable areas increase under all scenarios, with expansions ranging from +4.34% to +5.00% in the 2050s, +4.73% to +5.02% in the 2070s, and +4.84% to +5.00% in the 2090s.

Under current conditions, high, moderate, and low suitability represent 27.48%, 33.70%, and 38.82% of the total suitable area, respectively. Across future scenarios, the internal composition shifts toward moderate suitability, which increases to values between approximately 41.08% (e.g., 2050s SSP1–2.6) and 45.29% (e.g., 2090s SSP3–7.0). High suitability fluctuates between 24.55% (e.g., 2050s SSP5–8.5) and 30.14% (e.g., 2050s SSP2–4.5), while low suitability declines proportionally in most scenarios, ranging between 27.28% (e.g., 2050s SSP2–4.5) and 33.21% (e.g., 2050s SSP1–2.6). These patterns indicate a redistribution of suitable area toward intermediate agroclimatic conditions.

At the national scale, high suitability decreases from 3.28% of Peru under current conditions to values between 1.91% (e.g., 2050s SSP5–8.5) and 2.52% (e.g., 2050s SSP2–4.5) across future scenarios. Moderate suitability (4.03%) remains relatively stable, ranging from 3.22% (e.g., 2050s SSP1–2.6) to 3.63% (e.g., 2070s SSP1–2.6), while low suitability declines from 4.64% to between 2.28% (e.g., 2050s SSP2–4.5) and 2.60% (e.g., 2050s SSP1–2.6). Conversely, unsuitable areas expand from 83.04% at present to approximately 86.64%–87.21% of the national territory across all future scenarios. In addition to the net area changes observed for each period (Table 2), the transition maps and change matrices reveal the internal redistribution among suitability classes, showing how areas shift between high, moderate, low, and unsuitable categories under future scenarios (Figure 9).

Under current conditions, high suitability covers 42,322.95 km² (Table 2). Of this area, between 18,496.40 and 24,327.43 km² (43.7%–57.5%) remain stable as high suitability across future scenarios and periods (Figure 9). However, substantial portions transition to lower classes: between 15,766.88 and 20,373.60 km² (37.3%–48.1%) shift to moderate suitability, 1,816.23 to

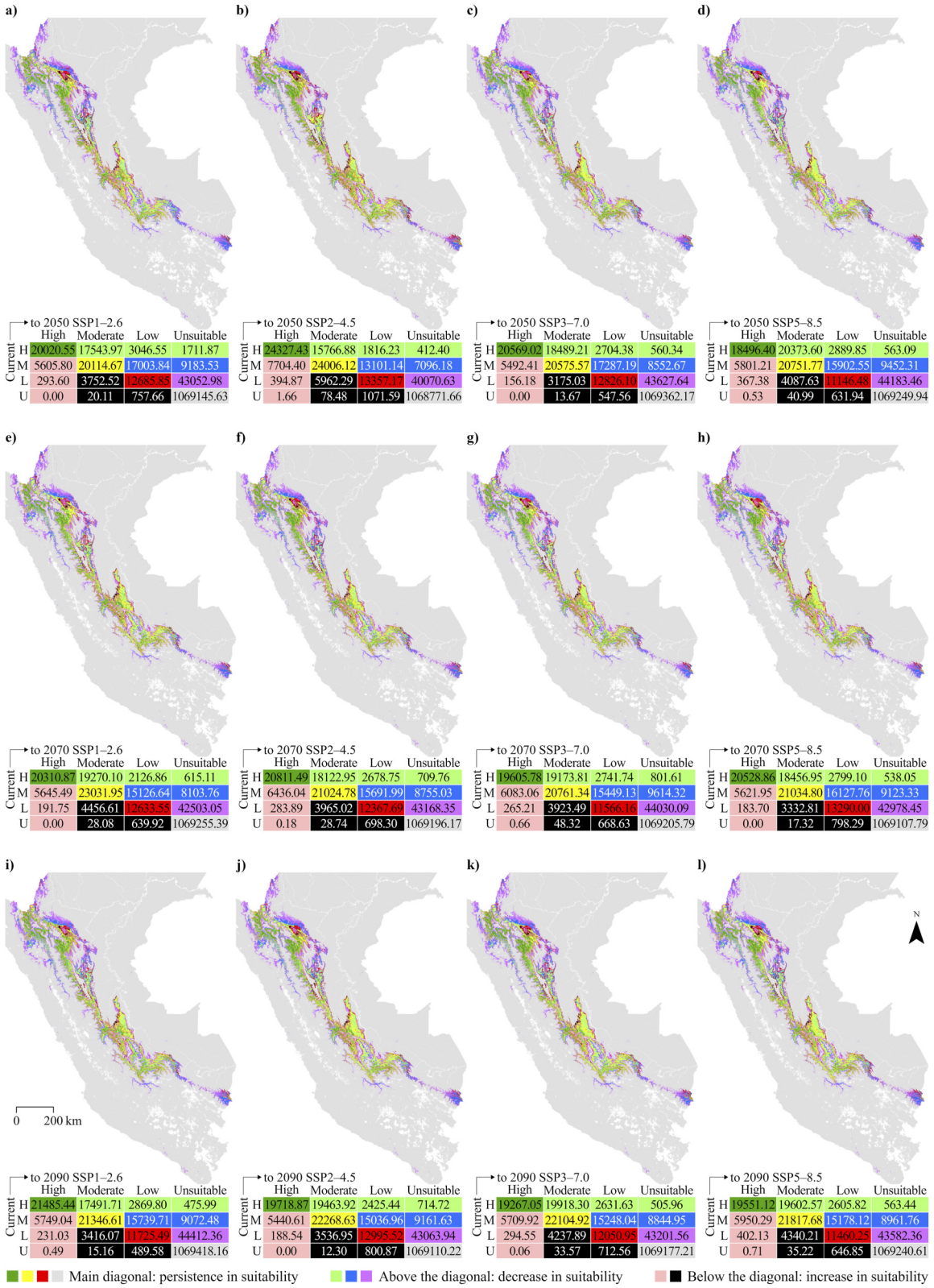

a) to 2050 SSP1–2.6	High	Moderate	Low	Unsuitable
H	20020.55	17543.97	3046.55	1711.87
M	5605.80	20114.67	17003.84	9183.53
L	293.60	3752.52	12685.85	43052.98
U	0.00	20.11	757.66	1069145.63

b) to 2050 SSP2–4.5	High	Moderate	Low	Unsuitable
H	24327.43	15766.88	1816.23	412.40
M	7704.40	24006.12	13101.14	7096.18
L	394.87	5962.29	13357.17	40070.63
U	1.66	78.48	1071.59	1068771.66

c) to 2050 SSP3–7.0	High	Moderate	Low	Unsuitable
H	20569.02	18489.21	2704.38	560.34
M	5492.41	20575.57	17287.19	8552.67
L	156.18	3175.03	12826.10	43627.64
U	0.00	13.67	547.56	1069362.17

d) to 2050 SSP5–8.5	High	Moderate	Low	Unsuitable
H	18496.40	20373.60	2889.85	563.09
M	5801.21	20751.77	15902.55	9452.31
L	367.38	4087.63	11146.48	44183.46
U	0.53	40.99	631.94	1069249.94

e) to 2070 SSP1–2.6	High	Moderate	Low	Unsuitable
H	20310.87	19270.10	2126.86	615.11
M	5645.49	23031.95	15126.64	8103.76
L	191.75	4456.61	12633.55	42503.05
U	0.00	28.08	639.92	1069255.39

f) to 2070 SSP2–4.5	High	Moderate	Low	Unsuitable
H	20811.49	18122.95	2678.75	709.76
M	6436.04	21024.78	15691.99	8755.03
L	283.89	3965.02	12367.69	43168.35
U	0.18	28.74	698.30	1069196.17

g) to 2070 SSP3–7.0	High	Moderate	Low	Unsuitable
H	19605.78	19173.81	2741.74	801.61
M	6083.06	20761.34	15449.13	9614.32
L	265.21	3923.49	11566.16	44030.09
U	0.66	48.32	668.63	1069205.79

h) to 2070 SSP5–8.5	High	Moderate	Low	Unsuitable
H	20528.86	18456.95	2799.10	538.05
M	5621.95	21034.80	16127.76	9123.33
L	183.70	3332.81	13290.00	42978.45
U	0.00	17.32	798.29	1069107.79

i) to 2090 SSP1–2.6	High	Moderate	Low	Unsuitable
H	21485.44	17491.71	2869.80	475.99
M	5749.04	21346.61	15739.71	9072.48
L	231.03	3416.07	11725.49	44412.36
U	0.49	15.16	489.58	1069418.16

j) to 2090 SSP2–4.5	High	Moderate	Low	Unsuitable
H	19718.87	19463.92	2425.44	714.72
M	5440.61	22268.63	15036.96	9161.63
L	188.54	3536.95	12995.52	43063.94
U	0.00	12.30	800.87	1069110.22

k) to 2090 SSP3–7.0	High	Moderate	Low	Unsuitable
H	19267.05	19918.30	2631.63	505.96
M	5709.92	22104.92	15248.04	8844.95
L	294.55	4237.89	12050.95	43201.56
U	0.06	33.57	712.56	1069177.21

l) to 2090 SSP5–8.5	High	Moderate	Low	Unsuitable
H	19551.12	19602.57	2605.82	563.44
M	5950.29	21817.68	15178.12	8961.76
L	402.13	4340.21	11460.25	43582.36
U	0.71	35.22	646.85	1069240.61

FIGURE 9
Future redistribution and transition matrices of suitable areas for *Coffea arabica* under various climate change scenarios. **(a)** To 2050 SSP1-2.6 **(b)** To 2050 SSP2-4.5 **(c)** To 2050 SSP3-7.0 **(d)** To 2050 SSP5-8.5 **(e)** To 2070 SSP1-2.6 **(f)** To 2070 SSP2-4.5 **(g)** To 2070 SSP3-7.0 **(h)** To 2070 SSP5-8.5 **(i)** To 2090 SSP1-2.6 **(j)** To 2090 SSP2-4.5 **(k)** To 2090 SSP3-7.0 **(l)** To 2090 SSP5-8.5.

3,046.55 km^2 (4.3%–7.2%) to low suitability, and 412.40 to 1,711.87 km^2 (1.0%–4.0%) to unsuitable conditions. Although high suitability experiences surface gains from moderate suitability, ranging between 5,440.61 and 7,704.40 km^2, and marginally from low suitability (156.18–402.13 km^2) and unsuitable areas (generally <2 km^2), these gains do not compensate for the larger downward transitions, resulting in a consistent net contraction of the high-suitability class ranging from −23.38% to −41.72%.

Moderate suitability (51,907.84 km^2 under current conditions) shows intermediate stability, with 20,114.67 to 24,006.12 km^2 (38.8%–46.2%) persisting as moderate (Figure 9). Upward transitions to high suitability range between 5,440.61 and 7,704.40 km^2 (10.5%–14.8%). In contrast, between 13,101.14 and 17,287.19 km^2 (25.2%–33.3%) decline to low suitability, and 7,096.18 to 9,614.32 km^2 (13.7%–18.5%) become unsuitable. Area gains to moderate suitability occur from low suitability, ranging between 3,175.03 and 5,962.29 km^2, and marginally from unsuitable areas (12.30–78.48 km^2). Despite these compensatory inflows, including substantial transfers from high suitability (15,766.88–20,373.60 km^2), the combined losses frequently exceed gains in several scenarios, resulting in a net contraction of the moderate-suitability class ranging from −9.87% to −20.18%, and reinforcing the pattern of internal redistribution rather than expansion of favorable conditions.

Of the low suitability area (59,784.95 km^2 under current conditions), between 11,146.48 and 13,357.17 km^2 (18.6%–22.3%) remain stable across scenarios (Figure 9), while substantial areas deteriorate to unsuitable conditions, ranging from 40,070.63 to 44,412.36 km^2 (67.0%–74.3%). Smaller proportions shift upward to moderate suitability (3,175.03–5,962.29 km^2; 5.3%–10.0%) and marginally to high suitability (156.18–402.13 km^2; <1%); however, despite surface gains from moderate (13,101.14–17,287.19 km^2) and high suitability (1,816.23–3,046.55 km^2), the dominant transitions toward unsuitable areas result in a consistent net contraction of the low-suitability class (−43.98% to −50.91%), confirming it as the most structurally unstable class under projected climate change.

Unsuitable areas expand primarily through inflows from suitable classes. The largest contribution comes from low suitability (40,070.63–44,412.36 km^2), followed by moderate suitability (7,096.18–9,614.32 km^2) and smaller transfers from high suitability (412.40–1,711.87 km^2). In contrast, upward transitions from unsuitable to any suitable class are minimal (≤1,071.59 km^2 across scenarios). This asymmetry explains the consistent net expansion of the unsuitable class, ranging from +4.34% to +5.02% relative to current conditions.

The relative persistence of high suitability area under future climate scenarios reveals a generalized decline across most coffee-producing departments (Figure 10). Among the seven departments with more than 3,600 km^2 of highly suitable land under current conditions, Cajamarca (73.5%–82.7%) and Junín (69.2%–80.3%, reaching 93.1% in 2050s SSP2–4.5) exhibit comparatively higher stability; Pasco (53.2%–74.8%, with 85.6% only in 2050s SSP2–4.5), San Martín (56.8%–75.4%) and Amazonas (61.3%–74.3%) show intermediate persistence; whereas Cusco (40.1%–66.6%) and Huánuco (49.1%–60.2%, with 75.2% only in 2050s SSP2–4.5) display comparatively lower persistence across several scenarios. Ucayali, which initially had ~1,600 km^2 of highly suitable land, shows the lowest persistence overall (14.9%–46.4%, with 54.2% only in 2050s SSP2–4.5). Among the eight departments with <850 km^2 of highly suitable area, Ayacucho shows moderate persistence (20.7%–46.0%, reaching 65.4% only in 2050s SSP2–4.5); La Libertad maintains low-to-moderate persistence (23.1%–41.7%); Piura ranges widely (16.7%–75.5%); whereas Loreto (0.4%–3.1%), Ancash (0.4%–0.7%), and Puno (0.0%) display an almost complete loss of high suitability across scenarios. Madre de Dios averages 74.8% persistence, although three outliers increase its variability. Huancavelica is the only department that increases its high-suitability area (176.1%–284.2%), reflecting expansion from a very limited baseline area.

4 Discussion

4.1 Biophysical determinants and spatial dynamics of coffee agroclimatic suitability

This study provides a robust assessment of the current and future potential distribution of *Coffea arabica* in Peru using the MaxEnt modeling framework, highlighting the dominant influence of key environmental drivers—particularly elevation, precipitation of the driest quarter (Bio17), soil nitrogen content, and soil pH in water. The convergence between Jackknife regularized gain analyses and variable contribution metrics reinforces the ecological relevance of these predictors, consistent with findings reported for tropical coffee-growing regions in Africa, Asia, and Latin America (Avalos et al., 2023; Benti et al., 2022; Li et al., 2024).

The unimodal response of *C. arabica* to elevation, with optimal suitability between 1,500 and 2,000 m a.s.l., aligns with observations from Mozambique (Cassamo et al., 2023) and Colombia (González-Orozco et al., 2024), where intermediate elevations provide favorable thermal regimes and relatively stable water availability. Likewise, precipitation during the driest quarter emerged as a critical determinant of suitability, supporting evidence from Ethiopia (Chalchissa et al., 2022) and China (Zhang et al., 2022), which emphasize the sensitivity of coffee phenology to seasonal water stress.

Edaphic variables further refined habitat suitability patterns. Soil nitrogen content and bulk density (bdod) played a substantial role in defining optimal conditions, corroborating studies in agroforestry systems in Peru (Haro et al., 2025) and Brazil (Gomes et al., 2020), where soil fertility and structure strongly influence coffee productivity and resilience. Although soil pH in water contributed less to overall model performance, its response curve indicated positive effects within acidic ranges, consistent with findings showing enhanced micronutrient availability under slightly acidic conditions (Abdelwahab et al., 2024).

At the national scale, under current climatic conditions (1970–2000), highly suitable areas represent approximately 3.3% of Peru's territory (42,322.95 km^2), primarily concentrated along the eastern Andean slopes. However, the progressive incorporation of spatial constraints reveals a pronounced funnel effect in effective land availability. Under Case 1 (exclusion of biophysical barriers), highly suitable areas constitute the baseline. In Case 2 (additional exclusion of legally protected areas), retention remains substantial in key producing departments, preserving the Andean–Amazonian gradient. In contrast, Case 3 (exclusion of forest cover consistent

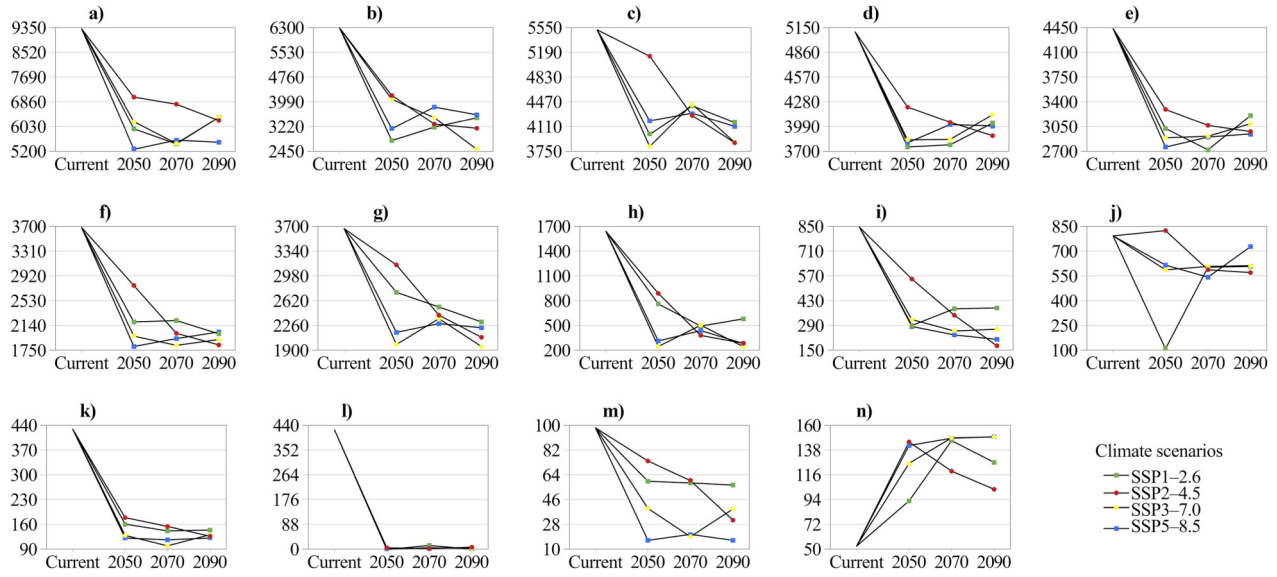

FIGURE 10
Change analysis in the high potential habitat distribution of coffee by department between the current scenario and future projections. **(a)** San Martín **(b)** Cusco **(c)** Junín **(d)** Cajamarca **(e)** Amazonas **(f)** Huánuco **(g)** Pasco **(h)** Ucayali **(i)** Ayacucho **(j)** Madre de Dios **(k)** La Libertad **(l)** Loreto **(m)** Piura **(n)** Huancavelica.

with EUDR criteria) produces the sharpest contraction, with reductions exceeding 80% in multiple territories and retention below 41% in 14 of the 16 departments that initially contained highly suitable areas. Finally, Case 4 (combined exclusion of protected areas, forest cover, and degraded lands) confirms that forest cover constitutes the principal limiting factor, as additional reductions relative to Case 3 are marginal (<1.3 percentage points in most departments). These results indicate that future territorial availability for sustainable coffee expansion in Peru is constrained less by formal protected-area designation than by the need to prevent deforestation in natural forests. This finding has direct implications for sustainable intensification and restoration-oriented strategies.

Under future climate scenarios (SSP1–2.6 to SSP5–8.5), projections indicate internal redistribution rather than expansion of the ecological niche. Highly suitable areas decline between −23.38% and −41.72% by mid-century, with sustained reductions toward the end of the century. Concurrently, moderately suitable areas increase proportionally within the suitable category, suggesting structural downgrading rather than abrupt disappearance. This pattern aligns with widely documented upward altitudinal shifts under warming scenarios (IPCC, 2022; de Sousa et al., 2019).

Transition matrices show that a substantial proportion of currently highly suitable areas shift toward moderate suitability, while low-suitability areas exhibit the greatest instability, with dominant transitions toward unsuitable conditions. This asymmetry explains the consistent expansion of unsuitable territory at the national level (+4.34% to +5.02%).

Although localized gains are projected in currently marginal regions (e.g., specific sectors of Piura or high-Andean zones), these gains do not compensate for losses within the principal production corridor. Therefore, adaptation cannot rely solely on geographic displacement but must incorporate resilience-based management strategies (Attiogbé et al., 2022; Bilen et al., 2023).

The intersection between high suitability and degraded lands adds a strategic dimension: approximately 39.8% of highly suitable areas overlap with degraded categories (low, medium, or high degradation). This finding supports the feasibility of productive restoration schemes aimed at reducing pressure on primary forests, consistent with global restoration frameworks (Griscom et al., 2017; Strassburg et al., 2020).

While integrating forest-cover exclusions enhances alignment with the European Union Deforestation Regulation (EUDR), it is essential to distinguish between modeled biophysical suitability and socio-institutional feasibility. Factors such as land tenure security, traceability systems, enforcement capacity, and economic incentives may condition the effective implementation of deforestation-free production strategies (European Commission, 2023).

4.2 Implications for public policy and territorial planning

The results obtained have direct implications for the design of climate adaptation strategies in the Peruvian coffee sector, as they identify territories that maintain high agroclimatic suitability under both current and future scenarios (Campos-Trigoso J. et al., 2025). These areas represent priority zones for investment in sustainable management practices, the strengthening of agroforestry systems, and the adoption of heat- and drought-tolerant varieties, which are widely recognized as key adaptation measures for climate-sensitive perennial crops (Bilen et al., 2023).

From a land-use planning and land-use policy perspective, the spatial differentiation between territories that are robust and those that are highly sensitive to climate change provides a solid scientific basis for guiding decisions on the expansion, intensification, or

restriction of coffee cultivation. In Andean–Amazonian regions, where altitudinal gradients generate high environmental heterogeneity, this type of information is essential for harmonizing productive objectives, ecosystem conservation, and climate risk reduction (Haro et al., 2025; Socolar et al., 2025).

Likewise, the progressive incorporation of exclusion scenarios—protected areas, forest cover, and degraded lands—allows the translation of ecological modeling results into concrete inputs for the implementation of deforestation-free supply chains. Recent studies demonstrate that identifying suitable areas outside natural forests is a central component for meeting traceability and sustainability standards required by international markets, without increasing pressure on forest ecosystems (Pendrill et al., 2019).

Finally, the spatial remnants identified under the most restrictive scenario, where high agroclimatic suitability converges with degraded lands, highlight priority opportunities for productive restoration. This approach enables the integration of climate adaptation objectives, landscape restoration, and rural development, aligning with global restoration strategies and with the need to strengthen the resilience of tropical agricultural systems (Griscom et al., 2017; Strassburg et al., 2020).

5 Conclusion

This study confirms that the ecological distribution of Coffea arabica in Peru is primarily determined by key environmental factors, particularly altitude, precipitation of the driest quarter, and edaphic properties such as soil nitrogen content and bulk density. It also demonstrates the robustness of the MaxEnt approach for modeling agroclimatic suitability across complex environmental gradients. The high model performance (AUC >0.85), together with the use of verified occurrence records and high-resolution environmental predictors, supports the accurate identification of areas with the highest climatic and edaphic suitability for crop establishment and development, providing relevant evidence-based information for agroecological planning.

Under current climatic conditions, highly suitable areas are mainly concentrated along the eastern slopes of the Andes, particularly in the departments of San Martín, Cajamarca, Amazonas, Cusco, Junín, and Pasco, which constitute the country's main coffee-producing corridors. Scenario-based spatial analyses reveal a pronounced funnel effect in the territorial availability of highly suitable areas, which becomes more pronounced as environmental and land-use restrictions are incorporated. This pattern makes it possible to distinguish territories that are relatively robust to climate change from those where productive restoration and sustainable management strategies are a priority.

Future climate projections under SSP1–2.6 to SSP5–8.5 scenarios indicate a spatial redistribution of agroclimatic suitability, characterized by a progressive upslope shift toward higher elevations and a gradual contraction of some currently productive zones. Although new potential areas are identified, their viability will depend on the effective implementation of adaptation strategies, investments in infrastructure, sustainable soil management, and the development of climate-resilient varieties.

Among the main limitations of this study is the reliance on climate projections derived from a single general circulation model, which introduces uncertainty associated with inter-model variability. Nevertheless, the evaluation of multiple SSP scenarios and the integration of climatic, topographic, and edaphic variables help mitigate this bias and strengthen the robustness of the results.

An additional limitation of this study relates to model evaluation metrics. Model performance was primarily assessed using the Area Under the Curve (AUC), a metric widely applied in presence-only species distribution models but known to have limitations, including limited sensitivity to model calibration and dependence on the extent of the background area. Although complementary diagnostics—such as omission rate analysis, assessment of predictor importance using the jackknife test, and the application of regularization to reduce overfitting and evaluate model robustness—were employed, additional threshold-dependent or calibration-oriented metrics (e.g., TSS or the continuous Boyce index) were not explicitly included. Future studies could incorporate these complementary metrics to further refine model evaluation, particularly in applications requiring binary suitability classifications or management threshold definition.

Overall, this study provides spatially explicit and scientifically robust evidence to support territorial planning, public policy design, and the development of climate adaptation strategies aimed at strengthening the resilience of the Peruvian coffee sector in the face of climate change.

Data availability statement

The original contributions presented in the study are included in the article/supplementary material, further inquiries can be directed to the corresponding authors.

Author contributions

JZ-S: Writing – original draft, Writing – review and editing, Conceptualization, Data curation, Formal Analysis, Investigation, Methodology, Resources, Software, Validation, Visualization. NR-B: Conceptualization, Software, Writing – original draft, Writing – review and editing. JS-L: Data curation, Methodology, Writing – original draft. AM-M: Methodology, Visualization, Writing – review and editing. KT-T: Methodology, Software, Writing – review and editing. AR-F: Formal Analysis, Validation, Writing – review and editing. TS-M: Methodology, Writing – review and editing. MG-A: Data curation, Writing – review and editing. JP-R: Software, Validation, Writing – review and editing. RS: Investigation, Supervision, Writing – review and editing. MO-C: Project administration, Resources, Supervision, Writing – review and editing. AC-S: Formal Analysis, Investigation, Methodology, Writing – review and editing. DG-F: Conceptualization, Methodology, Visualization, Writing – review and editing. EB: Writing – review and editing, Funding acquisition, Investigation, Project administration, Supervision.

Funding

The author(s) declared that financial support was received for this work and/or its publication. This work was supported by the Public Investment Project "Establishment of a Geomatics and

Remote Sensing Laboratory at the National University Toribio Rodríguez de Mendoza of Amazonas" (GEOMÁTICA, CUI No. 2255626). Article processing charges were covered by the Vice-Rectorate for Research of the National University Toribio Rodríguez de Mendoza–UNTRM.

Acknowledgements

The authors acknowledge and appreciate the support of the INDES-CES of the National University Toribio Rodríguez of Mendoza of Amazonas (UNTRM).

Conflict of interest

The author(s) declared that this work was conducted in the absence of any commercial or financial relationships that could be construed as a potential conflict of interest.

Generative AI statement

The author(s) declared that generative AI was not used in the creation of this manuscript.

Any alternative text (alt text) provided alongside figures in this article has been generated by Frontiers with the support of artificial intelligence and reasonable efforts have been made to ensure accuracy, including review by the authors wherever possible. If you identify any issues, please contact us.

Publisher's note

References

Abdelwahab, S. I., Elhassan Taha, M. M., Jerah, A. A., Aljahdali, I. A., Oraibi, B., Alfaifi, H. A., et al. (2024). Coffee arabica research (1932–2023): performance, thematic evolution and mapping, global landscape, and emerging trends. *Heliyon* 10 (16), 15. doi:10.1016/j.heliyon.2024.e36137

Adane, A. (2024). Analysis of current and future bioclimatic suitability for C. arabica production in Ethiopia. *PLoS ONE* 19 (10 October), 1–20. doi:10.1371/journal.pone.0310945

Alberto, N. J., Ferreira, A., Ribeiro-Barros, A. I., Aoyama, E. M., Silva, L. O. E., Rakocevic, M., et al. (2024). Plant morphological and leaf anatomical traits in coffea arabica L. cultivars cropped in gorongosa Mountain, Mozambique. *Horticulturae* 10 (9), 1–12. doi:10.3390/horticulturae10091002

Attiogbé, A. A. C., Abotsi, K. E., Adjossou, K., Parkoo, E. N., Adjonou, K., and Kokou, K. (2022). Climate vulnerability of coffee-cocoa agrosystems in the sub-humid Mountain ecosystems in south-west Togo (west Africa). *Environ. Syst. Res.* 11 (1), 15. doi:10.1186/s40068-022-00274-4

Avalos, A., Mar, S., Marceleño, L., Oyolsi, N., and Vilchez, F. F. (2023). "Potential coffee distribution in a central-western region of Mexico", *Ecologies* 4, 269–287. doi:10.3390/ecologies4020018

Avelino, J., Cristancho, M., Georgiou, S., Imbach, P., Aguilar, L., Bornemann, G., et al. (2015). The coffee rust crises in Colombia and central America (2008–2013): impacts, plausible causes and proposed solutions. *Food Secur.* 7 (2), 303–321. doi:10.1007/s12571-015-0446-9

Barboza, E., Bravo, N., Cotrina-Sanchez, A., Salazar, W., Gálvez-Paucar, D., Gonzales, J., et al. (2024). Modeling the current and future habitat suitability of neltuma pallida in the dry forest of northern Peru under climate change scenarios to 2100. *Ecol. Evol.* 14 (8), 1–16. doi:10.1002/ece3.70158

Beche, D., Tack, A. J. M., Ango, T. G., Nemomissa, S., Lemessa, D., Warkineh, B., et al. (2024). Spatial variation in current and historical management of arabica coffee across forests in its Indigenous distribution. *Plants People Planet* 7, 215–228. doi:10.1002/ppp3.10580

Benti, F., Diga, G. M., Feyisa, G. L., and Tolesa, A. R. (2022). Modeling coffee (coffea arabica L.) climate suitability under current and future scenario in jimma zone, Ethiopia. *Environ. Monit. Assess.* 194 (4), 10661. doi:10.1007/s10661-022-09895-9

Bilen, C., El Chami, D., Mereu, V., Trabucco, A., Marras, S., and Spano, D. (2023). A systematic review on the impacts of climate change on coffee agrosystems. *Plants* 12 (1), 1–20. doi:10.3390/plants12010102

Booth, T. H. (2018). Why understanding the pioneering and continuing contributions of BIOCLIM to species distribution modelling is important. *Austral Ecol.* 43 (8), 852–860. doi:10.1111/aec.12628

Bourgoin, C., Verhegghen, A., Degrève, L., Ameztoy, I., Carboni, S., Colditz, R., et al. (2024). *Global map of forest cover 2020 - version 2*. European Commission: Joint Research Centre, JRC.

Brummitt, N., Araújo, A. C., and Harris, T. (2021). Areas of plant diversity—What do we know? *Plants People Planet* 3 (1), 33–44. doi:10.1002/ppp3.10110

Burbano-Cushica, B., and Flores-Chiriboga, A. (2022). Evaluación Del Cambio Climático En La Producción Del Café (Coffea Arabica L.) Al 2040 En Cotachi-Ecuador. *Univ. Técnica del Norte*.

Campos-Trigoso, A., Rituay, P., Meliza del Pilar, B. C., Ramos-Sandoval, R., Rosmery, R.-S., Guadalupe, G. A., et al. (2025). Observed (1979–2024) and projected (2030) climate trends in relation to farmers' perceptions in coffee cooperatives of northern Peru. *Agriculture*. 16, 1–27. doi:10.3390/agriculture16010057

Campos-Trigoso, J., Rituay, P., Aldea, C., Meliza del Pilar, B. C., García, L., and Ramos-Sandoval, R. (2025). "Sensitivity and adaptive capacity to climate change in organised coffee growers in Amazonas, Peru", *Sustainability* 17, 1–23. doi:10.3390/su172310666

Cárdenas, G. P., Bravo, N., Barboza, E., Salazar, W., Ocaña, J., Vázquez, M., et al. (2023). Current and future distribution of shihuahuaco (dipteryx spp.) under climate change scenarios in the central-eastern amazon of Peru. *Sustain. Switz.* 15 (10), 1–16. doi:10.3390/su15107789

Cassamo, C. T., Draper, D., Romeiras, M. M., Marques, I., Chiulele, R., Rodrigues, M., et al. (2023). "Impact of climate changes in the suitable areas for coffea arabica L. production in Mozambique: Agroforestry as an alternative management system to strengthen crop sustainability", *Agric. Ecosyst. Environ.* 346 1–16. doi:10.1016/j.agee.2022.108341

Chalchissa, F. B., Diga, G. M., and Tolossa, A. R. (2022). Modeling the responses of coffee (coffea arabica L.) distribution to current and future climate change in jimma zone, Ethiopia. *Sains Tanah* 19 (1), 19–32. doi:10.20961/stjssa.v19i1.54885

Chaulagain, D., Ray, R. L., Yakub, A. O., Same, N. N., Jong, J. P., Roh, W., et al. (2025). "Impacts of climate change on hydrological patterns and implications for hydroelectric power generation in khimti river basin, Nepal,"*Discov. Appl. Sci.* 7 1–21. doi:10.1007/s42452-025-07304-7

Chemura, A., Mudereri, B. T., Yalew, A. W., and Gornott, C. (2021). "Climate change and specialty coffee potential in Ethiopia,"*Sci. Rep.* 11 1–13. doi:10.1038/s41598-021-87647-4

Chen, J., Lin, Z., Lin, J., and Wu, D. (2024). Investigating the spatial distribution and influencing factors of non-grain production of farmland in south China based on MaxEnt modeling and multisource Earth observation data. *Foods* 13 (21), 1–17. doi:10.3390/foods13213385

Coronel-castro, E., Meza-mori, G., Pariente-mondragón, E., Haro, N., Tariq, A., Guzman, B. K., et al. (2025). Habitat suitability distribution of genus gynoxys cass. (asteraceae): an approach to conservation and ecological restoration of the andean flora in Peru. *Sustainability* 17 (2406), 1–19. doi:10.3390/su17062406

Cotrina, A., Rojas Briceño, N. B., Bandopadhyay, S., Ghosh, S., Torres Guzmán, C., Oliva, M., et al. (2021). Biogeographic distribution of cedrela spp. genus in Peru using maxent modeling: a conservation and restoration approach. *Diversity* 13 (6), 15. doi:10.3390/d13060261

Cotrina-sanchez, A., Guzman, B. K., Barboza, E., Oliva, M., Huaman-pilco, A. F., and Rojas-brice, N. B. (2026). Integrating agroecological suitability of cacao (Theobroma cacao L.) with biodiversity and land-use constraints in Peru. *Agric. Syst.* 233 (January), 1–11. doi:10.1016/j.agsy.2026.104637

de Sousa, K., van Zonneveld, M., Holmgren, M., Kindt, R., and Ordoñez, J. C. (2019). The future of coffee and cocoa agroforestry in a warmer mesoamerica. *Sci. Rep.* 9 (1), 1–9. doi:10.1038/s41598-019-45491-7

Dormann, C. F., Elith, J., Bacher, S., Buchmann, C., Carl, G., Carré, G., et al. (2013). Collinearity: a review of methods to deal with it and a simulation study evaluating their performance. *Ecography* 36 (1), 27–46. doi:10.1111/j.1600-0587.2012.07348.x

Elith, J., Phillips, S. J., Hastie, T., Dudík, M., Chee, Y. E., and Yates, C. J. (2011). A statistical explanation of MaxEnt for ecologists. *Divers. Distributions* 17 (1), 43–57. doi:10.1111/j.1472-4642.2010.00725.x

European Commission (2023). European parliament and council of the european union. *Regul. (EU) 2023/1115 Eur. Parliam. Counc. 31 May 2023 Mak. Available Union Mark. Export Union Certain Commod. Prod. Assoc. Deforestation For. Degrad. And.* Available online at: https://eur-lex.europa.eu/eli/reg/2023/1115/oj/eng (Accessed September 17, 2025).

European Commission (2024). *Reglamento sobre productos libres de deforestación - comisión Europea*.

European Commission (2025). Regulation on deforestation-free products. *Energy, Clim. Change, Environ.* Available online at: https://environment.ec.europa.eu/topics/forests/deforestation/regulation-deforestation-free-products_en?utm_source=chatgpt.com (Accessed October 12, 2025).

Eyring, V., Bony, S., Meehl, G. A., Senior, C. A., Stevens, B., Stouffer, R. J., et al. (2016). Overview of the coupled model intercomparison project phase 6 (CMIP6) experimental design and organization. *Geosci. Model Dev.* 9 (5), 1937–1958. doi:10.5194/gmd-9-1937-2016

Fain, S. J., Quiñones, M., Álvarez-Berríos, N. L., Parés-Ramos, I. K., and Gould, W. A. (2018). Climate change and coffee: assessing vulnerability by modeling future climate suitability in the Caribbean island of Puerto Rico. *Clim. Change* 146 (1–2), 175–186. doi:10.1007/s10584-017-1949-5

Farr, T. G., Rosen, P. A., Caro, E., Crippen, R., Duren, R., Hensley, S., et al. (2007). The shuttle radar topography mission. *Geophys* 45, 1–33. doi:10.1029/2005RG000183

Feng, X., Park, D. S., Liang, Y., Pandey, R., and Papeş, M. (2019). Collinearity in ecological niche modeling: confusions and challenges. *Ecol. Evol.* 9 (July), 10365–10376. doi:10.1002/ece3.5555

Fick, S. E., and Hijmans, R. J. (2017). WorldClim 2: new 1-km spatial resolution climate surfaces for global land areas. *Int. J. Climatol.* 37 (12), 1–14. doi:10.1002/joc.5086

Fitzgibbon, A., Pisut, D., and Fleisher, D. (2022). Evaluation of maximum entropy (maxent) machine learning corn suitability. *Land*. 11, 1–20. doi:10.3390/land11091382

García, L., Laderach, P., and Posada, H. (2018). Evaluación del cambio de aptitud del cultivo del café en Colombia por variación en escenarios climáticos futuros. *Cenicafé* 69 (1), 91–111.

Gomes, L. C., Bianchi, F. J. J. A., Cardoso, I. M., Fernandes, R. B. A., Filho, E. I. F., and Schulte, R. P. O. (2020). Agroforestry systems can mitigate the impacts of climate change on coffee production: a spatially explicit assessment in Brazil. *Elsevier* 294 (February), 1–11. doi:10.1016/j.agee.2020.106858

Gómez-Fernández, D., Atalaya-Marin, N., Arce-Inga, M., Tineo, D., Fernandez-Jibaja, J. A., Taboada-Mitma, V. H., et al. (2025). Territorial zoning as a strategy for sustainable natural resource management in Cajamarca, northwestern Peru. *Ecol. Inf.* 92 (July), 103440. doi:10.1016/j.ecoinf.2025.103440

Gong, L., Li, X., Wu, S., and Jiang, L. (2022). Prediction of potential distribution of soybean in the frigid region in China with MaxEnt modeling. *Ecol. Inf.* 72, 101834. doi:10.1016/j.ecoinf.2022.101834

González-Orozco, C. E., Porcel, M., Byrareddy, V. M., Rahn, E., Cardona, W. A., Velandia, D. A. S., et al. (2024). Preparing Colombian coffee production for climate change: integrated spatial modelling to identify potential robusta coffee (coffea canephora P.) growing areas. *Clim. Change* 177 (4), 1–26. doi:10.1007/s10584-024-03717-2

Griscom, B. W., Adams, J., Ellis, P. W., Houghton, R. A., Lomax, G., Miteva, D. A., et al. (2017). Natural climate solutions. *PNAS* 114 (44), 11645–11650. doi:10.1073/pnas.1710465114

Haro, N., Meza-Mori, G., Zuta Lopez, J. L., Rascón, J., Pariente, E., Condori-Apfata, J. A., et al. (2025). Influence of agroforestry systems on coffea arabica L. yield and quality at different altitudes in Amazonas, Peru. *J. Agric. Food Res.* 19 (May), 1–13. doi:10.1016/j.jafr.2024.101574

Hou, Q., Bian, G., Jin, S., Song, H., and Bai, H. (2025). Prediction of potential suitable habitats for Liriomyza sativae blanchard in China under climate change scenarios. *Sci. Rep.* 15, 1–13. doi:10.1038/s41598-025-18273-7

Intergovernmental Panel on Climate Change (IPCC) (2022). Climate change 2022: impacts, adaptation and vulnerability. Available online at: https://www.ipcc.ch/report/ar6/wg2/ (Accessed October 31, 2023).

Jiang, F., Zhang, J., Gao, H., Cai, Z., Zhou, X., Li, S., et al. (2020). Musk deer (moschus spp.) face redistribution to higher elevations and latitudes under climate change in China. *Sci. Total Environ.* 704, 1–11. doi:10.1016/j.scitotenv.2019.135335

Jones, C. D., Arora, V., Friedlingstein, P., Bopp, L., Brovkin, V., Dunne, J., et al. (2016). C4MIP-The coupled climate-carbon cycle model intercomparison project: experimental protocol for CMIP6. *Geosci. Model Dev.* 9 (8), 2853–2880. doi:10.5194/gmd-9-2853-2016

Kamath, V., Sassen, M., Arnell, A., Soesbergen, A. V., and Bunn, C. (2024). "Agriculture, ecosystems and environment identifying areas where biodiversity is at risk from potential cocoa expansion in the Congo Basin", *Agric. Ecosyst. Environ.* 376, pp. 1–12. doi:10.1016/j.agee.2024.109216

Koutouleas, A., Sarzynski, T., Bordeaux, M., Bosselmann, A. S., Campa, C., Etienne, H., et al. (2022). Shaded-coffee: a nature-based strategy for coffee production under climate change? A review. *Front. Sustain. Food Syst.* 6 (April), 1–21. doi:10.3389/fsufs.2022.877476

Lahai, P. M., Aikpokpodion, P. O., Bah, A. M., Lahai, M. T., Meinhardt, L. W., Lim, S., et al. (2025). Unveiling the genetic diversity and demographic history of coffea stenophylla in Sierra Leone using genotyping-by-sequencing. *Plants* 14 (1), 1–18. doi:10.3390/plants14010050

Lara-Estrada, L., Rasche, L., and Schneider, U. A. (2021). Land in central America will become less suitable for coffee cultivation under climate change. *Reg. Environ. Change* 21 (3), 1–13. doi:10.1007/s10113-021-01803-0

Li, S., Wang, Z., Zhu, Z., Tao, Y., and Xiang, J. (2023). Predicting the potential suitable distribution area of Emeia pseudosauteri in Zhejiang Province based on the MaxEnt model. *Sci. Rep.* 13 (1), 1–11. doi:10.1038/s41598-023-29009-w

Li, X., Wang, Z., Wang, S., and Qian, Z. (2024). MaxEnt and marxan modeling to predict the potential habitat and priority planting areas of coffea arabica in Yunnan, China under climate change scenario. *Front. Plant Sci.* 15 (November), 1–21. doi:10.3389/fpls.2024.1471653

Liu, X., Tan, Y., Dong, J., Wu, J., Wang, X., and Sun, Z. (2025). Assessing habitat selection parameters of arabica coffee using BWM and BCM methods based on GIS. *Sci. Rep.* 15 (1), 1–19. doi:10.1038/s41598-024-84073-0

Mendes, G. de A., de Oliveira, M. A. L., Rodarte, M. P., de Carvalho dos Anjos, V., and Bell, M. J. V. (2022). Origin geographical classification of green coffee beans (coffea arabica L.) produced in different regions of the Minas Gerais state by FT-MIR and chemometric. *Curr. Res. Food Sci.* 5, 298–305. doi:10.1016/j.crfs.2022.01.017

Merow, C., Smith, M. J., and Silander, J. A. (2013). A practical guide to MaxEnt for modeling species' distributions: what it does, and why inputs and settings matter. *Ecography* 36 (March), 1–12. doi:10.1111/j.1600-0587.2013.07872.x

Ministerio de Desarrollo Agrario y Reigo (MIDAGRI) (2023). *El Café Peruano"*, Ministerio de Desarrollo. Available online at: https://www.midagri.gob.pe/portal/485-feria-scaa/10775-el-cafe-peruano (Accessed November 23, 2023).

Ministerio del ambiente (MINAM) (2019a). *Mapa Nacional de Áreas Degradadas En Ecosistemas Terrestres*. Available online at: https://catalogo.geoidep.gob.pe/metadatos/srv/api/records/88eab65d-202f-4452-a1b0-2c45fb60e0a2 (Accessed November 24, 2025).

Ministerio del Ambiente (MINAM) (2019b). *Mapa nacional de ecosistemas*. Available online at: https://sinia.minam.gob.pe/mapas/mapa-nacional-ecosistemas-peru (Accessed November 26, 2025).

Ministerio del Ambiente (MINAM) (2025). Intercambio de datos – Geoservidor. Available online at: https://geoservidor.minam.gob.pe/recursos/intercambio-de-datos/ (Accessed September 17, 2025).

Ministerio del Ambiente (MINAM) (2026). Bosque y pérdida de bosque: Geobosques. *Geobosques*. Available online at: https://geobosques.minam.gob.pe/geobosque/view/descargas.php?122345gxxe345w34gg#download (Accessed February 15, 2026).

Muscarella, R., Galante, P. J., Soley-guardia, M., Boria, R. A., Kass, J. M., and Anderson, R. P. (2014). *ENMeval: an R package for conducting spatially independent evaluations and estimating optimal model complexity for M AXENT ecological niche models*, 1198–1205. doi:10.1111/2041-210X.12261

Ortega, S., Páez, G. T., Feria, T. P., and Muñoz, J. (2017). Climate change and the risk of spread of the fungus from the high mortality of Theobroma cocoa in Latin America. *Taylor and Francis* 3 (1), 30–40. doi:10.1080/23766808.2016.1266072

Ovalle-Rivera, O., Läderach, P., Bunn, C., Obersteiner, M., and Schroth, G. (2015). Projected shifts in coffea arabica suitability among major global producing regions due to climate change. *PLoS ONE* 10 (4), 1–13. doi:10.1371/journal.pone.0124155

O'Neill, B. C., Tebaldi, C., Van Vuuren, D. P., Eyring, V., Friedlingstein, P., Hurtt, G., et al. (2016). The scenario model intercomparison project (ScenarioMIP) for CMIP6. *Geosci. Model Dev.* 9 (9), 3461–3482. doi:10.5194/gmd-9-3461-2016

Parada-Molina, P. C., Cerdán-Cabrera, C. R., Cervantes-Pérez, J., Barradas, V. L., and Ortiz-Ceballos, G. C. (2025). Impact of climate on water status, growth, yield, and phenology of coffee (coffea arabica) plants in the central region of the state of Veracruz, Mexico. *PLoS ONE* 20 (4 APRIL), 1–18. doi:10.1371/journal.pone.0319670

Pendrill, F., Persson, U. M., Godar, J., Kastner, T., Moran, D., Schmidt, S., et al. (2019). Agricultural and forestry trade drives large share of tropical deforestation emissions. *Glob. Environ. Change* 56, 1–10. doi:10.1016/j.gloenvcha.2019.03.002

Phillips, S. J., and Miroslav, D. (2008). Modeling of species distributions with maxent: new extensions and a comprehensive evaluation. *Ecography* 7 (1), 161–175. doi:10.1038/s41597-019-0343-8

Phillips, S. J., Dudík, M., and Schapire, R. E. (2004). "A maximum entropy approach to species distribution modeling," in Proceedings, twenty-first international conference on machine learning, ICML 2004, 655–662. doi:10.1145/1015330.1015412

Phillips, S. B., Aneja, V. P., Kang, D., and Arya, S. P. (2006). Maximum entropy modeling of species geographic distributions. *Int. J. Glob. Environ. Issues* 6 (2–3), 231–252. doi:10.1016/j.ecolmodel.2005.03.026

Phillips, S. J., Anderson, R. P., Dudík, M., Schapire, R. E., and Blair, M. E. (2017). Opening the Black box an open-source release of maxent. *Ecography* 40, 887–893. doi:10.1111/ecog.03049

Poggio, L., De Sousa, L. M., Batjes, N. H., Heuvelink, G. B. M., Kempen, B., Ribeiro, E., et al. (2021). SoilGrids 2.0: producing soil information for the globe with quantified spatial uncertainty. *Soil* 7 (1), 217–240. doi:10.5194/soil-7-217-2021

Promnun, P., Kongrit, C., Tandavanitj, N., Techachoochert, S., and Khudamrongsawat, J. (2020). Predicting potential distribution of an endemic butterfly lizard, Leiolepis ocellata (squamata: agamidae). *Trop. Nat. Hist.* 20 (1), 60–71. doi:10.58837/tnh.20.1.198819

Purba, P., Sukartiko, A. C., and Ainuri, M. (2019). Modeling the plantation area of geographical indication product under climate change: Gayo arabica coffee (coffea arabica). *IOP Conf. Ser. Earth Environ. Sci.* 365 (1), 1–10. doi:10.1088/1755-1315/365/1/012021

R Core Team. (2020). "*A language and environment for statistical computing*", R Foundation for Statistical Computing: Vienna, Austria, Available online at: https://www.r-project.org/ (Accessed 30 June 2025).

Rabelo de Oliveira, K., Marques Ferreira, W., Miranda, V., De Fátima Souza, C., and Castro Ribeiro, A. (2018). Identificação Das Áreas Potenciais de Expansão Do Café Na Região Das Matas de Minas, Estado de Minas Gerais, Brasil, IX Congresso Ibérico de Agroengenharia. *Univ. Fed. Viçosa*.

Radosavljevic, A., and Anderson, R. P. (2014). Making better M AXENT models of species distributions: complexity, overfitting and evaluation. *J. Biogeogr.* 41, 629–643. doi:10.1111/jbi.12227

Rojas-Briceño, N. B., Cotrina-Sánchez, D. A., Barboza-Castillo, E., Barrena-Gurbillón, M. ángel, Sarmiento, F. O., Sotomayor, D. A., et al. (2020). Current and future distribution of five timber forest species in Amazonas, northeast Peru: contributions towards a restoration strategy. *Diversity* 12 (8), 1–21. doi:10.3390/D12080305

Rojas-Briceño, N. B., García, L., Cotrina-Sánchez, A., Goñas, M., Salas López, R., Silva López, J. O., et al. (2022). Land suitability for cocoa cultivation in Peru: AHP and MaxEnt modeling in a GIS environment. *Agronomy* 12 (12), 20. doi:10.3390/agronomy12122930

Rojas-Briceño, N. B., Cajas-Bravo, V., Pasquel-Cajas, A., Guzman, B. K., Silva-López, J. O., Veneros, J., et al. (2025). Effectiveness of protected areas in containing the loss of Peruvian Amazonian forests. *Trees, For. People* 19 (January), 1–11. doi:10.1016/j.tfp.2025.100778

Salas, R., Gómez, D., Silva López, J. O., Rojas Briceño, N. B., Oliva, M., Terrones Murga, R. E., et al. (2020). Land suitability for coffee (Coffea arabica) growing in Amazonas, Peru: integrated use of AHP, GIS and RS. *ISPRS Int. J. Geo-Information* 9 (11), 1–21. doi:10.3390/ijgi9110673

Servicio Nacional de Áreas Naturales Protegidas por el Estado (SERNANP) (2023). Patrimonio Natural Del Perú*, 2da edició*.

Servicio Nacional de Áreas Naturales Protegidas por el Estado (SERNANP) (2025). "GEO ANP-Visor de Areas naturales Protegidas," in *GEO ANP - visor de Las Áreas Naturales Protegidas*. Available online at: https://geo.sernanp.gob.pe/visorsernanp/ (Accessed September 17, 2025).

Servicio Nacional de Meteorología e Hidrología (SENAMHI) (2022). Mapa Climático del Perú. Available online at: https://www.senamhi.gob.pe/mapas/mapa-climatico-v2/ (Accessed August 10, 2025).

Shcheglovitova, M., and Anderson, R. P. (2013). Estimating optimal complexity for ecological niche models: a jackknife approach for species with small sample sizes. *Ecol. Model.* 269, 9–17. doi:10.1016/j.ecolmodel.2013.08.011

Socolar, J. B., Mills, S. C., Gilroy, J. J., Martínez-revelo, D. E., Medina-uribe, C. A., Parra-sanchez, E., et al. (2025). Tropical biodiversity loss from land-use change is severely underestimated by local-scale assessments. *Nat. Ecol. and Evol.* 9 (September), 1643–1655. doi:10.1038/s41559-025-02779-4

Strassburg, B. B. N., Iribarrem, A., Beyer, H. L., Cordeiro, C. L., Crouzeilles, R., Jakovac, C. C., et al. (2020). Global priority areas for ecosystem restoration. *Nature* 586 (7831), 724–729. doi:10.1038/s41586-020-2784-9

Sun, S., Zhang, Y., Huang, D., Wang, H., Cao, Q., Fan, P., et al. (2020). The effect of climate change on the richness distribution pattern of oaks (quercus L.) in China. *Sci. Total Environ.* 744, 1–12. doi:10.1016/j.scitotenv.2020.140786

UNEP and FAO (2021). "United nations decade on ecosystem restoration (2021–2030)," in *Ecosystem restoration*, 1–6.

United States Agency for International Development (USAID) (2017). *Climate change risk in Peru: country risk profile*", ATLAS, 5.

Wang, S., Lu, Y., Han, M., Li, L., He, P., Shi, A., et al. (2023). "Using MaxEnt model to predict the potential distribution of three potentially invasive scarab beetles in China", *Insects* 14, 1–12. doi:10.3390/insects14030239

Wigoberto Alvarado, C., Bobadilla, L. G., Valqui, L., Valqui, G. S., Valqui-Valqui, L., Vigo, C. N., et al. (2022). Characterization of coffea arabica L. parent plants and physicochemical properties of associated soils, Peru. *Heliyon* 8 (10), 1–8. doi:10.1016/j.heliyon.2022.e10895

World Bank (2020). As peru's agricultural production grows, smallholders long for better markets. Available online at: https://blogs.worldbank.org/latinamerica/peru-s-agricultural-production-grows-smallholders-long-better-markets (Accessed October 31, 2023).

Wu, J., Wei, X., Wang, Z., Peng, Y., Liu, B., and Zhuo, Z. (2024). Mapping the distribution of Curculio davidi fairmaire 1878 under climate change *via* geographical data and the MaxEnt model (CMIP6). *Insects* 15 (8), 1–15. doi:10.3390/insects15080583

Yang, J., Id, P. J., Huang, Y., Yang, Y., Wang, R., and Id, Y. Y. (2022). Potential geographic distribution of relict plant Pteroceltis tatarinowii in China under climate change scenarios. *PLOS ONE*, 17, 1–21. doi:10.1371/journal.pone.0266133

Zhang, S., Liu, X., Li, R., Wang, X., Cheng, J., Yang, Q., et al. (2021). AHP-GIS and MaxEnt for delineation of potential distribution of arabica coffee plantation under future climate in Yunnan, China. *Ecol. Indic.* 132, 108339. doi:10.1016/j.ecolind.2021.108339

Zhang, S., Liu, B., Liu, X., Yuan, Q., Xiao, X., and Zhou, T. (2022). Maximum entropy modeling for the prediction of potential plantation distribution of arabica coffee under the CMIP6 mode in Yunnan, southwest China. *Atmosphere* 13 (11), 1773. doi:10.3390/atmos13111773